IRis

Northeastern University

Civil Engineering Master's Theses

Department of Civil and Environmental Engineering

January 01, 2011

Evaluating steel-reinforced concrete bridge decks using ground-penetrating radar: models for deterioration

Christopher Franklin Wright
Northeastern University

Recommended Citation

Wright, Christopher Franklin, "Evaluating steel-reinforced concrete bridge decks using ground-penetrating radar: models for deterioration" (2011). *Civil Engineering Master's Theses.* Paper 14. http://hdl.handle.net/2047/d20001042

This work is available open access, hosted by Northeastern University.

EVALUATING STEEL-REINFORCED CONCRETE BRIDGE DECKS USING GROUND-PENETRATING RADAR: MODELS FOR DETERIORATION

A Thesis Presented

by

Christopher Franklin Wright

to

The Department of Civil and Environmental Engineering

in partial fulfillment of the requirements

for the degree of

Master of Science

in

Civil Engineering

Northeastern University

Boston, Massachusetts

April 2011

Abstract

Lack of regular maintenance programs for infrastructure systems in the United States has created a sizeable financial gap between available and required funds to keep these essential systems in good condition. Asset management strategies are being employed to ensure the most efficient use of available funds. Bridges, and their decks in particular, are components of the infrastructure system that are well suited for management by these systems due to their accessibility and general uniformity. Essential to successful bridge management is knowledge of the current state of the bridge network as well as the ability to forecast future states. Several nondestructive testing technologies have the potential to fill this role and among them, Ground Penetrating Radar (GPR) stands out as an efficient and easy to use tool.

Ground penetrating radar faces several challenges before it can become an integral part of bridge management systems and the most important of these is to increase the accuracy with which it can detect corrosion in steel reinforced concrete bridge decks. This issue has been addressed through computational modeling of bridge deck conditions that lead to anomalies in GPR data often correlated with damage in the deck. Two models were examined: one representing an early stage of deterioration where contaminants are concentrated in the concrete covering the steel reinforcement, and the other a later stage of deterioration where the reinforcement is surrounded by contaminants. Simulations with both models resulted in GPR responses that could be interpreted as damage. Since only one of the models directly affected the reinforcing steel, it was concluded that this was a likely source of errors in GPR diagnoses. A better understanding of how GPR responds to all stages of deterioration can contribute to the development of data analysis techniques that minimize these errors while boosting overall efficiency.

Acknowledgements

This thesis was directly supported by the doctoral training program in Intelligent Diagnostics for Aging Civil Infrastructure Systems supported by National Science Foundation Grant Number: DGE - 0654176. The work was indirectly supported by Gordon-CenSSIS, the Bernard M. Gordon Center for Subsurface Sensing and Imaging Systems, under the Engineering Research Centers Program of the National Science Foundation (Award Number EEC-9986821). I appreciate these sources of funding and am especially grateful for their flexibility to allow the exploration of multiple research topics.

Thank you to Kim Belli for the use of your software as well as your technical support. Your time, patience, and thoughtful suggestions were immensely helpful and much appreciated. Thank you to Abhijit Ganguli for your interest in this project and help in collecting experimental data. Thank you to Michael MacNeil for your help with setting up experiments. Thank you to Ken Maser for lending your equipment, advice, and vast experience to this project.

Thank you to my advisers, Sara Wadia-Fascetti and Carey Rappaport, for your guidance, expertise, and enthusiasm toward this project. Amidst your myriad activities you always made time for me and I can't thank you enough for your wisdom and contributions. Thank you also to Dennis Bernal for giving me the opportunity to explore other areas of Intelligent Diagnostics before settling on the topic presented herein.

Thank you to Julie Van Deusen for your incredible support and for teaching me about split infinitives, commas, and hyphens.

Contents

Chapter 1: Introduction

Once a source of pride for the United States, the infrastructure system that holds such a prominent place in history is quickly entering a state of disrepair. The current infrastructure, which includes the entire transportation network, power grid, water supply, and waste management systems, was given a grade of D in a 2009 review by the American Society of Civil Engineers (ASCE). In their evaluation, the ASCE estimates that $2.2 trillion must be invested over the next five years to return the system to respectable standing (ASCE, 2009). While the infrastructure crisis is often referred to as one massive problem, many contest that due to the diversity of systems under the infrastructure umbrella, there are really a number of problems that each require a unique solution. Following that logic, this thesis closely examines one such problem: the large number of deficient bridges in the United States. The potential solution considered here is the development of NonDestructive Testing (NDT) technologies that can provide the information necessary to make smart, cost effective decisions that will restore reliability and serviceability to bridges. Before addressing this subject directly, it is helpful to consider the origins of NDT and how it has revolutionized other industries.

1.1 Broader Impact of Nondestructive Testing

The American Society for Nondestructive Testing (ASNT) defines NDT as any technique or method used to examine an object, material, or system without impairing its future usefulness (ASNT, 2011). Under this definition, NDT includes a vast number of methods with applications that range from authenticating artwork to searching for oil deep within the earth's crust. The most basic method is visual inspection, which has been in use since the beginning of recorded history. While fundamental theories and archaic practices were in place before the 1920's, it was during this decade that several NDT methods still used today began to gain momentum (Hellier, 2003). Forerunners of the magnetic particle test, liquid penetrant test, and X-radiography were all present at this time, although their applications were

extremely limited. It was reported as recently as the mid 1990's that magnetic particle and liquid penetrant tests account for about 50%, X-radiography and ultrasonics about 33%, and eddy current methods about 10% of NDT in the engineering industry (Cartz, 1995). These technologies as well as others saw unprecedented development during and after World War II, when resources were channeled toward technological innovation (Hellier, 2003). More recent advances in NDT technology are largely due to the advent of powerful computing and data storage technology (Hellier, 2003). The ability to process and analyze huge amounts of data automatically has opened avenues that could not previously be explored.

While many NDT methods have resulted from landmark technical innovations, there are some that work on basic human sensory capabilities. Despite the wide range of complexity, NDT technologies all work on the same basic principle. They must identify and measure a physical phenomenon that can interact with the specimen in question without altering it in a meaningful way (Shull, 2002). The more sensitive the physical phenomenon is to relevant changes in the specimen, the more effective the technique. For example, in evaluating concrete bridge decks, the physical phenomena might be radar waves interacting with the deck. Based on an understanding of how radar waves interact with concrete, the condition of the deck's subsurface can be inferred. This highlights another common theme in NDT—that in most cases the parameter in question is not being directly interrogated. Rather, the physical phenomena must be interpreted to indirectly infer the state of the parameter.

The inherent inability of NDT to directly assess a parameter in question has led to many general misconceptions. It is often the case that too much is expected from NDT because the limitations and sources of error are not fully understood. One prevalent belief is that NDT methods are magical cure-alls that eliminate defects and failures (Hellier, 2003). Every NDT technology has limitations and understanding what capabilities and certainties can be associated with NDT is crucial to their successful

implementation. Part of this comes from the fact that the results of NDT are rarely definitive in an absolute sense. The consequence of this is that judgments based on NDT data often rely heavily on statistics to establish thresholds between normal and abnormal behavior. The method used to establish these thresholds, as well as the uncertainties that accompany them, are sources of error that keep NDT from being 100% reliable.

It is also the exceptional case that one NDT method can evaluate all types of defects or modes of failure for a system or component (Hellier, 2003). For example, the evaluation of an airplane part may employ one NDT method to look for surface defects and another to look for internal discontinuities. Still another factor that affects the reliability of NDT is the personnel involved with the evaluation process (Hellier, 2003). Experience, mental and physical ability, fatigue, and attitude can all play a role in the accuracy and thoroughness of NDT results.

Despite these misconceptions, NDT has become an essential component in most major industries because of its ability to decrease risk. The motivations for minimizing risk can be evaluated based on the consequences of failure. The most serious of these involve safety issues and loss of human life. Large systems and safety-critical components are evaluated more rigorously than those whose failures pose little risk to human life (Shull, 2002). Aircraft, power plants, and bridges fall into this category and extensive NDT programs are implemented to evaluate them, often with government regulation and oversight. One strategy used to extend the life of large and expensive systems in known as Retirement-for-cause, where a system that is older than its design life continues to operate after extensive NDT determines that it is safe and productive (Shull, 2002). Another strategy is known as Risk-informed and works to strategically concentrate NDT and inspections on components with high probabilities and dire consequences of failure (Shull, 2002).

While preventing accidents and saving lives are the most important reasons for utilizing NDT, profit for the user is probably the most common (ASNT, 2011). Consistently manufacturing a product that works reliably and performs up to the standard expected by the customer is a challenging task where NDT takes a central role. Success in this area is crucial to the good reputation and growth of many businesses.

Nondestructive testing had become essential to manufacturing because the increase in complexity of devices has been accompanied by increased expectations of the consumer. On a basic level, a manufacturer may determine that a critical system component fails 1 time in 100. While this may be an acceptable rate of failure, if a system is made up of 10 such components, the probability of failure is $0.99^{10} = 0.904$, or nearly 10% (ASNT, 2011). This highlights the need to ensure the quality of each component and helps justify the investment in NDT. In addition, NDT can aid in the design process, help to control and lower manufacturing costs, and maintain uniform quality.

There are many cases where NDT has revolutionized and transformed an industry. Many early experts in NDT were focused on applications in medicine and the technology has advanced to a point where many consider medical diagnostics to be a field of its own. The ability to noninvasively image bone and tissue structure has fueled advances leading to routine procedures that are used to treat what were once debilitating or lethal conditions. The X-ray started this diagnostic revolution and led to the development of the computer-aided tomography scan, magnetic resonance imaging, and ultrasound (Shull, 2002). The development of techniques and equipment for medical applications continues to dominate the cutting edge of NDT research.

As previously mentioned, many NDT technologies were developed because of their military applications during World War II. One reason for this is that military equipment must remain operable in some of the harshest environments and therefore requires a level of reliability above and beyond that provided by

standard manufacturing processes. Another is the strategic advantage that sensor systems can provide on enemy position, terrain, and hidden infrastructure. Since then, the defense industry has developed and added to these capabilities to such an extent that they have transformed the way wars are fought and funded. Going even further, these transformations have affected the political proceedings that lead to conflict as well as the general public's perception of war.

There are also a multitude of NDT methods devoted to the evaluation of infrastructure, particularly roadways, bridges and buildings. These methods can be roughly divided into two groups based on the scope of their evaluations: local and global. A global method assesses the condition of an entire structure, such as a building or bridge. For example, structural health monitoring is a method that places sensors on a structure that measure its vibrations at a number of locations. The goal is to determine the condition of the structure by analyzing the vibrations. This information can be used to prevent catastrophic failures and to establish need-based maintenance programs that result in cost savings over the life of the structure.

Another set of methods look for localized damage and defects in components of structures. Most use various strategies to image subsurface conditions and look for abnormalities. Roadways and bridge decks are common subjects for evaluation with these techniques with the goal being to increase quality and safety while minimizing maintenance costs.

At this point the discussion is narrowed to look in detail at how NDT methods can impact bridges and their decks in particular. The strategies described are focused on bridge decks; however, the fundamental logic can be applied to a wide variety of NDT programs.

1.2 The State of U.S. Bridge Infrastructure

There are over 600,000 bridges in the United States, and, the majority of them were designed to last on the order of 50 years (ASCE, 2009). The U.S. Department of Transportation reports that bridges have an

average age of 43 years and this long service time has led to relatively poor ratings. Upon inspection, a bridge can receive one of several designations. Bridges deemed *structurally deficient* must post weight limits and are not unsafe unless the limits are exceeded. Bridges found to be *functionally obsolete* are also not unsafe, but are no longer able to carry the necessary volume of traffic and are often the root causes of congestion. Both designations indicate that the bridge cannot perform to modern requirements and that significant opportunities exist for improvement. In 2008, one in three urban bridges, and one in four rural bridges was classified as either structurally deficient or functionally obsolete. Critical ratings exist for bridges thought to be nearing collapse; however, these bridges account for a small fraction of the network and are closely monitored.

One of the major reasons for the generally poor state of bridges is the lack of regular preventative maintenance. Maintenance and rehabilitation programs are rarely advocated for and funded by politicians because they represent a continuation of the status quo, rather than the quantifiable improvement embodied by new construction projects. In addition, maintenance projects are often perceived negatively because they shut down lanes and add to traffic congestion and commuting times.

1.3 Infrastructure Management

Asset management strategies have been successfully utilized in many fields and ASCE advocates that these strategies be applied to bridges as part of its proposal for improving bridge conditions. A Bridge Management System (BMS) would serve to evaluate, predict, and prioritize work related to the maintenance and repair of bridges. The decks of bridges are the most vulnerable to deterioration because of direct exposure to weather, traffic loading, and chemical contamination. The vast majority of bridge deficiencies involve cracking, potholes, and other damage to the deck and in many cases the deck also functions as a crucial protector of the steel substructure. The vulnerability and importance of the deck make it the best suited component for management because it presents the greatest opportunity

for cost savings and quality improvement. Strategies for managing bridge assets can include other components, but are discussed here with a focus on bridge decks.

Since there isn't enough money to address all of the concerns, a BMS is necessary to make decisions that bring the most benefit per dollar invested. On a network level, a BMS can help decide which bridges to repair based on a desired average condition of the network and when to repair them to minimize their life cycle costs (Hegazy, Elbeltagi, & Elbehairy, 2004). A BMS can also work on a project level to help decide on the best repair option given a bridge's age, history, current condition and life cycle cost projections. Periodic and minor maintenance are the repair options that require the least amount of time and dollars. The investment increases with rehabilitation projects and complete bridge replacements. Early BMSs focused either on the network or project levels, but more recent work by Hegazy et al. (2004) has shown the success of a BMS that can integrate information at both levels.

Bridge management systems consist of three fundamental components or functions that must be tied together in a database: evaluation and inspection, modeling and prediction, and decision-making (Elbeltagi & Tantawy). The most common method for evaluating bridge decks, for which there are several standardized processes, is to perform a visual inspection and assign the bridge a numerical rating. While visual inspections are the cheapest and simplest, they are highly subjective and there is significant opportunity to improve upon them by integrating more advanced NDT methods into the process.

The success of a BMS depends heavily on the model used to forecast rates of deterioration and future bridge conditions. Models are typically formulated based on historical data, but the quality of the data as they relate to the real state of the bridges has a significant effect on decisions made by the BMS (Rens, Nogueira, & Transue, 2005). The model must not only predict deterioration over time, but also the effect of any repairs performed. Depending on the type of repair selected, the immediately

improved condition and eventual deterioration rate may vary. General models for deterioration and repair are depicted in Figure 1.1.

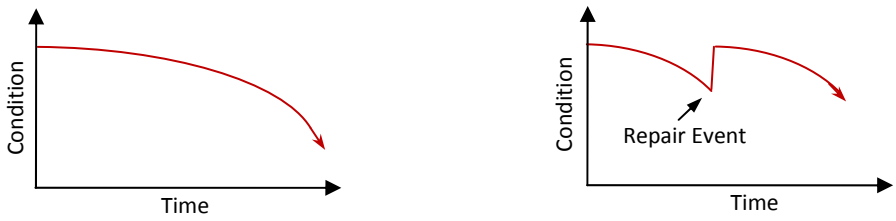

Figure 1.1: Illustrative models for deterioration of bridge decks over time

The decision-making component of a BMS is essentially an optimization problem with multiple user defined constraints. In the BMS described by Hegazy et al. (2004), inputs are defined over some period of time and include budget for repairs, desired average bridge rating, lowest absolute bridge rating, and number of desired visits to a given bridge for repair activities. In addition, one can input nonflexible actions, such as a bridge repair project that has already been planned. With so many constraints and variables, the problem becomes quite large, and is handled with a Genetic Algorithm. The output of the system is a year to year schedule describing which bridges to repair and how much to repair them in order to obtain the minimum desired ratings for the network. In a small case study, Hegazy et al. (2004) showed that the BMS suggestions resulted in a network rating over five years that significantly exceeded the minimum with a realistic budget. It was noted that the BMS most often suggested maintenance or rehabilitation projects rather than total replacement. This is because once deterioration begins, the overall condition of the bridge declines quickly (Rens et al., 2005). Periodic maintenance to prevent a bridge from entering this stage of rapid deterioration is a more cost effective approach over the life cycle of the bridge than waiting until total replacement is necessary.

1.4 The Role of NDT in Bridge Management

Nondestructive Testing has the potential to contribute to both the network and project levels of a BMS while improving the evaluation and forecasting components. On the network level, NDT can quantify the

total amount of deterioration present in the bridge network so that an appropriate amount of funding can be allocated for repairs. On a project level, NDT can locate deterioration in a given bridge deck and help decide on the best repair strategy. Once a repair project is decided on, this information encourages an efficient construction process and decreases the chances for cost overruns due to unanticipated damage. Work can be focused on deteriorated areas and lane closures can be minimized while maximizing the ride quality of the roadway over the service life of the bridge.

During the evaluation process, NDT can offer a wealth of information beyond what visual inspections provide. The ability to probe the subsurface of bridge decks introduces the possibility of identifying the precise location and severity of corrosion present there. This data can serve as a quantitative, objective complement to visual inspections. This new information also contributes to the formulation of more robust deterioration and forecasting models that form the basis of decisions made by a BMS.

In short, the implementation of a BMS that includes data from NDT could have a sizeable impact on how society views and uses transportation infrastructure. From the user's standpoint, regular maintenance means a higher quality product. A structure that is repaired when it reaches mediocre condition avoids the drastic decrease in quality experienced by structures that are allowed to deteriorate until replacement is necessary. A maintenance project can be performed in far less time than a complete bridge replacement and minimizes lane closures and other traffic delays. Most of all, a BMS that includes NDT data ensures the best use of taxpayer's dollars while minimizing waste and cost overruns.

1.5 NDT Technologies for Bridge Deck Inspection

Nondestructive Testing inspections are not currently a routine part of bridge management because they are too costly to perform over an entire network of bridges. For the additional time and dollars spent, NDT surveys do not necessarily guarantee better information than visual inspections and many bridge officials express a lack of confidence in the results. It is widely accepted that visual inspection should be

the default evaluation method. Until NDT becomes cheaper and more reliable, Rens et al. (2005) suggest that only a subset of bridges in a network be evaluated with NDT methods, while the others are visually inspected.

In this section, a number of NDT technologies with applications to bridge deck inspection are reviewed, with particular attention given to their drawbacks and potential for cost-effective use as part of a BMS. Fundamental principles employed by these technologies include acoustics, electromagnetics, and infrared.

1.5.1 Chain Drag

One of simplest NDT methods is the chain drag and is still commonly relied upon to identify areas of deterioration in reinforced concrete bridge decks. The chain drag is typically used to locate areas of deterioration in order to direct a repair effort, rather than to collect preliminary data as part of a BMS. The chain drag does not work on bridge decks with asphalt overlays, and, in these cases, does not become useful until the repair project is underway and the overlay has been removed. The survey involves dragging a chain over the bridge deck while an inspector listens for changes in pitch that represent deteriorated areas. The results of a chain drag survey are generally accepted as being accurate; however, it is slow, subjective, and results can vary depending on the experience of the inspector.

1.5.2 Impact-Echo

This test method induces stress waves in concrete using a small impact hammer and records the response using an accelerometer mounted next to the hammer. Recorded data is analyzed in the frequency domain, where cracks and delaminations can be identified. While the data is quantitative, the big drawback is that the survey is slow; it must be performed on a point by point basis over the testing area.

1.5.3 Half Cell Potential

The half cell potential is the only NDT method that directly measures corrosion activity (Rens et al., 2005). The electrical potential of the steel reinforcement is measured relative to a reference half cell on the surface (McCann & Forde, 2001). Active corrosion is indicated by high potential gradients. Areas of corrosion can be identified before delamination occurs but direct contact with the reinforcement is needed and requires drilling a small hole in the concrete, which makes the process slow. In addition, the half cell potential method does not work on bridge decks with asphalt overlays.

1.5.4 Infrared Thermography

It has been observed that anomalies under the surface of bridge decks change the way that heat flows through the deck. Using special cameras that pick up infrared heat signatures, bridge decks can be surveyed to look for these anomalies. Areas with cracks and delaminations will have a higher temperature during heating than areas of sound concrete. This method is fast, but requires that the surface be a constant color and texture. An additional weakness is that asphalt overlays can obscure anomalies in the underlying concrete.

1.5.5 Ground Penetrating Radar

Ground Penetrating Radar (GPR) stands out in its potential to be integrated into a BMS and is central to this thesis. Described in detail in Section 2.1, GPR employs electromagnetic (EM) waves to probe the subsurface of bridge decks and identify areas of increased moisture and chloride content that can correlate with deterioration. The promise of GPR rests on its ability to collect data while moving at traffic speeds, to both localize and quantify deterioration, and to perform well whether or not an asphalt overlay is present. The high rate of data collection calls for automated data processing and analysis. If done efficiently, this could alleviate part of the high cost generally associated with GPR that comes from the need to have experienced professionals interpreting the data by hand. There are also

issues related to the accuracy and reliability (See Section 2.3.3) of GPR that need to be addressed before the technology can take its place in a BMS.

One way to address some of the shortcomings of GPR for concrete bridge deck evaluations is through computational modeling of deterioration. The GPR response to a deteriorated section of concrete is generally accepted and recognizable. However, little attention has been paid to how these deteriorated sections develop, and to what their material properties are during this process. Before corrosion of the steel reinforcement begins, contaminants must penetrate from the surface to catalyze the chemical reaction. Understanding the deterioration process and GPR's response to it through modeling can aid in the development of accurate and efficient data analysis algorithms. Driven by data signatures that indicate damage in concrete bridge decks, this thesis examines what conditions may be present in those decks to produce these signatures and how they relate to the process of deterioration.

Chapter 2: Background

This chapter reviews the fundamental theories, technologies, and methodologies that play key roles in this work. First, an overview of GPR is given. Following that are reviews of the relevant material properties used for modeling and current techniques and challenges associated with using GPR to identify damage in bridge decks. Finally, the software used for computational modeling is reviewed and a derivation is given for the Finite Difference Time Domain algorithm.

2.1 Ground-Penetrating Radar

Ground-Penetrating Radar uses a transmitter to direct a pulse of electromagnetic (EM) energy into the subsurface. A receiver, often packaged in the same housing as the transmitter, records the reflected energy. Reflections occur at interfaces between materials with different EM properties. For each pulse

of the transmitter, the receiver records the strength of reflections and time at which they were received. The result is a time history of the reflection strength that is stored on a control unit connected to the antenna housing.

Figure 2.1: *Left*: Ground Coupled GPR antenna *Right*: Air Coupled GPR antenna (GSSI, 2011)

Antennas come in several variations depending on the application. Each antenna is either air or ground coupled. Air coupled antennas operate with the antenna housing held at some constant height above the surface (Figure 2.1 right). The overwhelming advantage of this setup is that the antenna can be mounted to a vehicle and moved over a surface at highway speeds while collecting data. For infrastructure applications, this means that lane closures are not required and that miles worth of data over roadways can be collected efficiently. One drawback is that since the antenna is held above the surface, a significant portion of the signal is reflected from the surface, which limits penetration depth. In addition, this allows the pulse to spread out before being transmitted to the surface, which can make it difficult to resolve individual targets.

Ground coupled antennas operate in direct contact with the surface (Figure 2.1 left). This allows for an efficient transmission of the excitation into the subsurface with relatively small energy losses from the surface reflection resulting in greater penetration depth. Contact with the surface does not allow space for the beam to spread out so finer resolution of targets is possible. The obvious drawback of a ground coupled antenna is that it must be dragged across the surface, substantially limiting its operating speed.

Another distinguishing property of antennas is the frequency at which they operate, usually between 90MHz and 2.6GHz (GSSI, 2011). The frequency is chosen based on the anticipated depth and size of the target. A high frequency antenna produces short wavelengths capable of resolving small targets but energy is dissipated quickly and the waves cannot penetrate deeply into the subsurface. Low frequency antennas transmit long waves that penetrate deeply but are not able to distinguish between small objects. The ideal application for antennas is this frequency range is the mapping of soil and rock layers.

For highway applications, air coupled antennas that operate between 1GHz and 2.6GHz are most commonly used because they offer fast data collection and their primary targets—steel reinforcing bars—are usually located only a few inches below the surface. In this study, detailed images of individual rebar are desired to evaluate how they appear in both healthy and deteriorated states. In the experimental components of this work, a 1.5GHz GSSI ground coupled antenna was used to obtain detailed images.

A typical GPR survey consists of collecting multiple lines of data over the survey area. The lines are often collected in a grid pattern, with the spacing determined by the specific application and smallest anticipated target. Antenna setups often make use of a survey wheel that measures the distance the antenna has traveled. The survey wheel also tells the antenna when to fire a pulse. For example, the antenna could be set to transmit a pulse six times for every foot of horizontal distance traveled. For each pulse, a time history of the reflection strength, or scan, is recorded. A typical scan recorded directly over a steel reinforcing bar is shown in Figure 2.2. The direct transmission is the signal that passes directly through the free space separating the transmitter and receiver. With a ground coupled antenna, the surface is close enough to the transmitter and receiver that the direct transmission and surface reflection combine and are recorded indistinguishably as the same signal. This fact eliminates methods used for calculating the material conditions on the surface that rely on measuring the surface reflection alone.

It should also be noted that the receiver itself has no concept of depth; it can record only the time at which a reflection was received. Calculations based on the material properties of the subsurface can be used to estimate the depth of targets as a function of time.

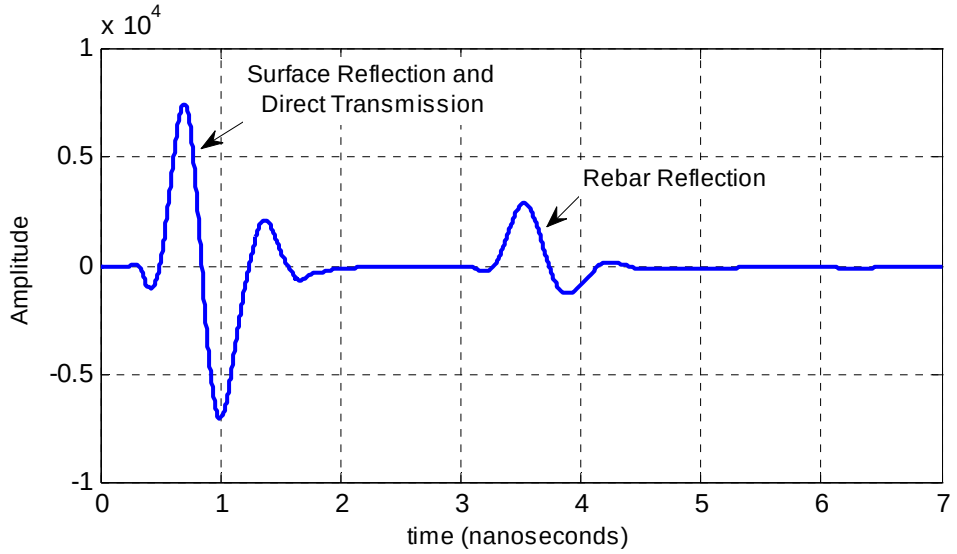

Figure 2.2: Typical scan, or time history of reflection amplitude, recorded by GPR over a reinforcing bar

Multiple scans can be assembled into a picture that displays the data for an entire line of GPR motion. This image is called a B-scan and consists of multiple scans arranged side by side such that the horizontal axis represents distance across the surface and the vertical axis represents time. The strength of the reflection is mapped to a color axis. For example, as the antenna approaches the target (Antenna Position 1 in Figure 2.3), the distance to the target d_1 is great, and so the scan at this position (Scan 1, Figure 2.4) shows the target reflection late in time and relatively weak in strength. The further a target is from the antenna, the more energy from the initial pulse is dissipated as the wave propagates, which results in a weaker reflection. When the antenna is positioned directly over the target (Antenna position 2 in Figure 2.3), the distance to the target d_2 is at a minimum and the target reflection shows up strong and early in time (Scan 2, Figure 2.4). As the antenna moves away from the target (Antenna position 3,

Figure 2.3), it is a mirror image of Antenna position 1 and the same scan will be collected as in position 1 (Scan 3, Figure 2.4). This will be true only if Antenna positions 1 and 3 are equidistant from the target.

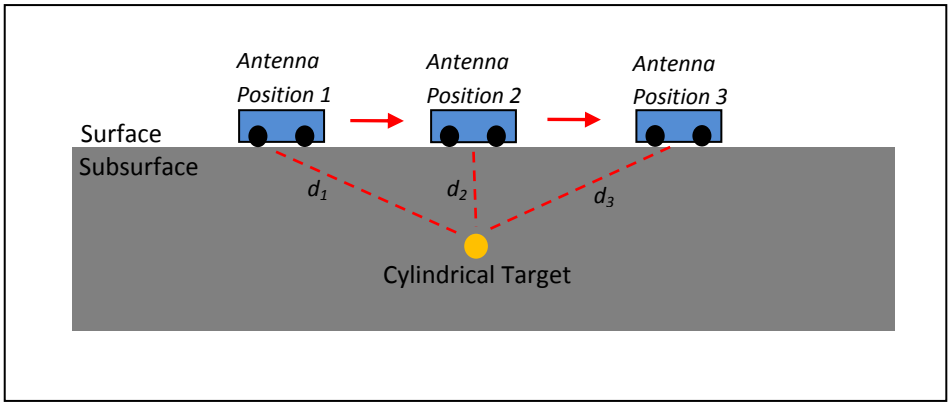

Figure 2.3: Three positions of a GPR antenna as it crosses a cylindrical target

As the antenna moves continuously over the target, many scans are collected and can be viewed together in a B-scan (Figure 2.5). Typical B-scans are in grayscale (although any color mapping scheme can be used) with white areas representing strong positive reflections and black regions indicating strong negative reflections. Shades of light and dark gray represent medium strength positive and negative reflections.

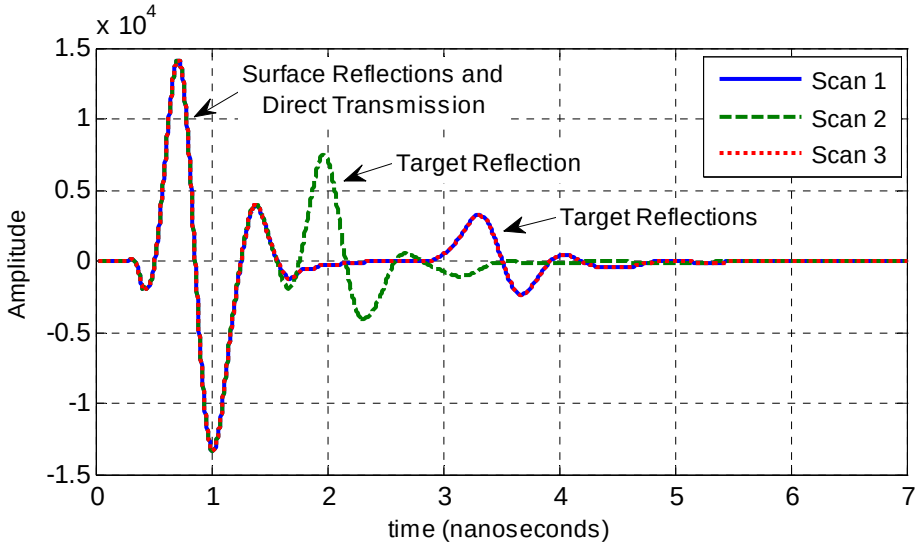

Figure 2.4: Scans recorded at the three antenna positions shown in Figure 2.3

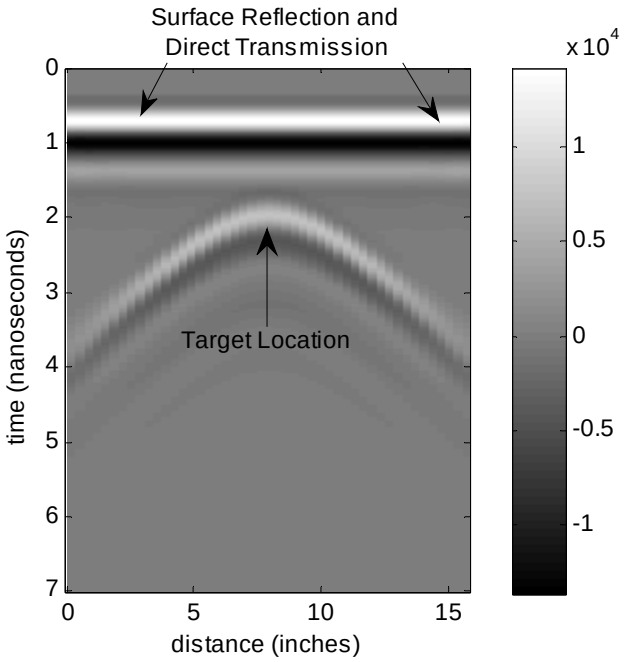

Figure 2.5: B-scan collected over a cylindrical metal target

2.2 Electromagnet Material Properties

Central to this study is an understanding of how the conditions in concrete that lead to the corrosion of the steel reinforcement alter reflections recorded by GPR. Changes to the material properties of concrete are insignificant in the view of GPR unless they change the way that EM waves propagate through the medium in an observable way. Common construction materials such as concrete and asphalt act as electrical insulators that can be polarized by an electric field and are known as dielectric materials. The behavior of EM waves within such mediums is controlled by two independent properties, the complex permittivity, ϵ^*, and the complex permeability, μ^*. In general, construction materials are nonmagnetic (as are most dielectrics), and thus the permeability has little effect on GPR reflections because the permeability within the material is very close to that of free space (Buyukozturk, 1997). Because of this, permittivity plays the biggest role and can be defined as

$$\epsilon^* = \epsilon' - j\epsilon'' \quad (2.1)$$

where ϵ' is the real part of the complex permittivity, ϵ'' is the imaginary part of the complex permittivity, and $j = \sqrt{-1}$. In general, the real part is responsible for the velocity with which waves travel, while the imaginary part controls the loss, or attenuation experienced by the wave. These effects are of particular interest because changes in the strength and time of arrival of reflections are two of the most commonly observed anomalies in GPR data. Due to the functionality of the simulation software, the properties used for modeling are the dielectric constant and the conductivity. These properties can be derived from, and are analogous to, the real and complex parts of the complex permittivity.

2.2.1 Dielectric Constant

Dividing Equation 2.1 by the permittivity of free space, $\epsilon_0 = 8.85 \times 10^{-12}$ farad/m, Equation 2.2 gives an analogous equation for the complex relative permittivity where the subscript r indicates a quantity relative to that of free space (Buyukozturk, 1997).

$$\frac{\epsilon^*}{\epsilon_0} = \frac{\epsilon'}{\epsilon_0} - \frac{j\epsilon''}{\epsilon_0}$$
$$\epsilon_r^* = \epsilon_r' - j\epsilon_r'' \quad (2.2)$$

The real quantity ϵ_r', henceforth ϵ_r, is unitless and is known as the relative permittivity or dielectric constant. The dielectric constant for air is 1 by definition. At a frequency of 3 GHz and room temperature, fresh water is reported to have a dielectric constant of 76.7 while a 0.3 molal salt water solution measures 69.3 (von Hippel, 1954). According to the Society of Exploration Geophysicists of Japan (1998), concrete construction materials have a dielectric constant that falls between 4 and 10 when dry, and between 10 and 20 when wet, (as cited in Belli, 2008, p. 23).

The velocity of an EM wave is dictated by the dielectric constant of the medium it is traveling through. When the medium is air, $\epsilon_r = 1$ and the velocity is the speed of light, $c = 3 \times 10^8$ m/sec. As the dielectric increases, the velocity, v, decreases according to Equation 2.3.

$$v = \frac{c}{\sqrt{\epsilon_r}} \tag{2.3}$$

The dielectric constant also has consequences for target detection with GPR. The wavelength, λ, depends on the velocity of the wave and the frequency of oscillation, f, as shown in Equation 2.4 (Buyukozturk, 1997).

$$\begin{aligned} \lambda &= \frac{1}{f} \times v \\ &= \frac{1}{f} \times \frac{c}{\sqrt{\epsilon_r}} \end{aligned} \tag{2.4}$$

Therefore, a wave of given length travelling in free space will see its wavelength shorten as it enters a material with a dielectric constant higher than 1. For successful target detection using GPR, the wavelength must be shorter than twice the target length (Buyukozturk, 1997). Higher dielectric constants would seem to aid target detection because they shorten the wavelength; however, there is a quantitative association of high dielectric constants with high loss factors. The result is high signal attenuation and limited penetration depth, which tends to diminish the advantage.

2.2.2 Conductivity

Attenuation of EM waves results from the generation of currents in the dielectric material that conduct the energy away. The measure of a material's ability to support these currents is known as the electrical conductivity, denoted by σ, and is expressed in Equation 2.5 using the imaginary part of the complex permittivity.

$$\sigma = \epsilon''(2\pi f) = \epsilon_r'' \epsilon_0 (2\pi f) \quad 2.5$$

At a frequency of 1.5 GHz, the conductivity of concrete ranges from being negligible when dry to around 0.1 Siemens/m when wet (Buyukozturk, 1997). Aqueous chloride ions present in saturated concrete can have a large effect on the conductivity depending on the frequency. Calculated from values reported by von Hippel (1954), the conductivities of fresh water and a 0.3 molal salt water solution at 300 MHz are 0.02 S/m and 2.84 S/m respectively. At 3 GHz, the conductivities are calculated as 2.01 S/m and 5.03 S/m for the same fresh and salt water. The estimated conductivity of concrete saturated with salt water depends on the concentration of chloride ions and the mixture model used to combine the properties of the solution and concrete. However, it is reasonable to assume that the presence of chloride ions in solution will significantly increase the conductivity of concrete.

2.3 Detecting Damage in Reinforced Concrete Bridge Decks

Many of the techniques developed to detect damage in concrete bridge decks using GPR depend on an understanding of what changes occur beneath the surface of the deck during active corrosion. Damage can only be successfully detected if the changes to the material properties of the bridge deck caused by corrosion also affect the way EM waves propagate and reflect in the medium. The following section reviews the deterioration process experienced by rebar in concrete bridge decks and covers the techniques and difficulties associated with detecting this deterioration using GPR.

2.3.1 The Process of Deterioration

Concrete is a porous medium and thus allows liquid and gaseous contaminants to penetrate into it. Steps can be taken to limit this penetration; however, over the lifecycle of the concrete, keeping contaminants from reaching steel reinforcement has not yet been achieved. Water, chloride ions from

deicing salts, and carbon dioxide from the atmosphere inevitably reach the steel and act as the catalysts for corrosion.

Steel is produced by smelting and refining iron ore—a process that adds energy to the metal (PCA, 2011). This added energy makes steel unstable under normal atmospheric conditions, with its tendency being to return to the lower energy state of iron oxide, commonly known as rust. Details of the chemical reaction are given by the Portland Cement Association (2011), but here it suffices to say that iron atoms become ionized and combine with water and oxygen through a series of oxidation and reduction reactions to form any of a number of iron oxides. These iron oxide molecules occupy two to four times the volume of the constituent iron atoms (NRMCA, 1995).

Though the corrosion reactions take place easily in the atmosphere, the conditions inside concrete actually work to protect the steel. Concrete is an alkaline (basic) environment with a pH typically in the 12-13 range (PCA, 2011). Under these conditions, a passive oxide layer forms on the outside of the steel and prevents the metal atoms from dissolving. Corrosion is not eliminated completely, but rather reduced to a rate at least 1,000 times slower than in the atmosphere (PCA, 2011). Exposure to contaminants works to destroy this protection and explains why concrete protected from the elements does not face the corrosion problems that occur in bridge decks.

The major contributor to the destruction of the passive protection layer that opens the door to corrosion is the presence of water soluble chloride ions (PCA, 2011). These chloride ions originate from deicing salts or seawater and reach the reinforcing steel by becoming dissolved in water that permeates the concrete through pores or cracks. While the mechanisms are not fully understood, the role of chloride ions in the corrosion process seems to be limited to the relatively easy penetration of the passive protection layer (PCA, 2011). Once this layer is penetrated, as long as water and oxygen are

present, corrosion can occur at an increased rate that depends only indirectly on the concentration of chlorides present.

Another process that affects the passive layer is known as carbonation. This happens when carbon dioxide from the atmosphere permeates the concrete and reacts with hydroxides to form carbonates (PCA, 2011). These reactions create molecules that reduce the pH of the concrete and cause the passive layer to become unstable. Carbonation has been estimated to move through high quality concrete at a rate of 1 mm per year, but this rate can be significantly influenced by cement-to-water ratios in the concrete, curing times, relative humidity of the concrete, and cracking or other weaknesses (PCA, 2011). Carbonation also decreases the concentration of the chlorides required to initiate corrosion, so it is likely the two work in tandem to break down the passive layer.

The effects of corrosion vary widely from case to case. As rust is produced, the surrounding concrete is stressed and becomes susceptible to cracking as a result of the increased volume. This eventually causes the rebar to debond from the concrete. This is especially an issue with pre-tensioned steel tendons, which keep the concrete in compression and support tensile loads. When the steel becomes debonded from the concrete, these tensile loads are transferred to the concrete, which does not have good strength characteristics under tension. This can lead to extensive cracking, potholes, and loss of overall structural integrity. Extensive horizontal cracking can also occur that entirely separates layers of concrete. This is known as a delamination and often results in a void space between the separated layers.

2.3.2 Detecting Deterioration with GPR

Techniques for detecting damage in reinforced concrete bridge decks revolve around the detection of increased moisture and chloride content in the concrete (Barnes & Trottier, 2004; Maser, 1996). While the notion exists that cracks, delaminations, and voids can be detected directly, multiple authors report

that this is impractical, and likely impossible, given the sub-millimeter to millimeter size of the cracks and the wavelengths of common GPR antennas in concrete (Barnes, Trottier, & Forgeron, 2008; Maser, 1996). In general, ground truth comparisons with GPR data substantiate these claims (Barnes & Trottier, 2000).

The approach then, is to detect symptoms of deterioration. As catalysts for corrosion, the presence of moisture and chlorides tends to correlate with cracking, delaminations, and other damage. Given enough time, these contaminants will eventually penetrate healthy concrete by way of either diffusion driven by electrochemical or concentration gradients, or by water seepage driven by hydraulic gradients (Gontar, Martin, & Popovics, 2000). Models for chloride penetration in concrete by these mechanisms have been developed both analytically and empirically (Nielson & Geiker, 2003; Xi & Bazant, 1999). If these mechanisms were wholly responsible for chloride and moisture penetration in bridge decks, one would expect uniform penetration to be a common occurrence, assuming that water and chloride are evenly distributed over the surface of the deck. Since uniformity is not often observed, the reasons for localized penetration must be considered. Few definitive claims have been reported, but Gontar et al. (2000) suggest that cyclical loading of a concrete member can have a significant effect on its porosity and chloride penetration through the member. This sort of loading may result from traffic on bridge decks. Other factors that may expedite penetration in some locations but not in others include ice buildup, freeze-thaw effects, poor quality concrete, thickness of the concrete cover layer, and depressions that allow puddles to form.

Ingress of moisture and chlorides into the concrete alters the GPR response in several obvious ways. In general, these two contaminants work to increase both the dielectric constant and conductivity of the concrete. Increases in these properties make the contrast between concrete and air stronger, which results in a larger reflection from the air-concrete (or in the presence of an asphalt overlay, the asphalt-

concrete) interface. This is known as increased surface reflectivity. Another indicator is the attenuation of reflections from the reinforcement due to the presence of aqueous chloride ions. Identifying these two effects (shown in Figure 2.6), either with an automated algorithm, or by visual inspection of the data, forms the basis of detecting damage in concrete bridge decks (Barnes & Trottier, 2000; Maser, 1996). Both of these indicators require establishment of a reference that represents sound concrete. Because of the variation in condition and construction of bridge decks, a reference is established for each deck rather than referring to a universal standard. Predictions of deterioration are made if surface reflectivity or attenuation is high in comparison to the reference. For this reason, large contrasts in radar signatures between sound and deteriorated areas lead to the most accurate identification of damage (Barnes & Trottier, 2004).

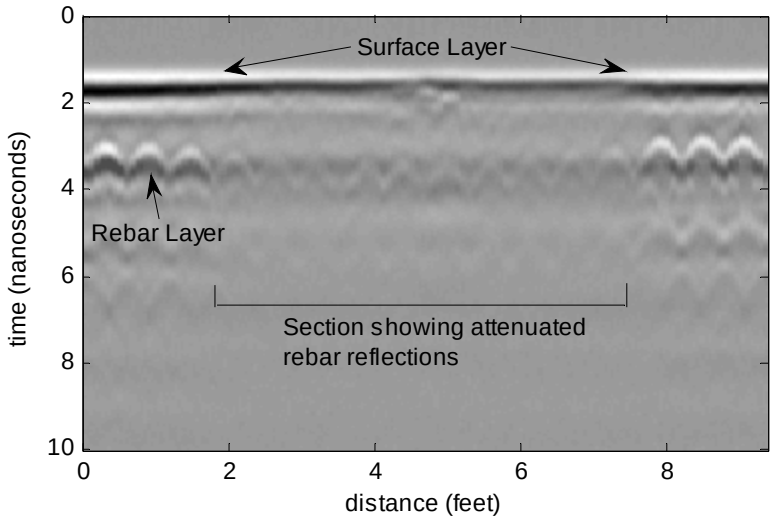

Figure 2.6: B-scan showing a potentially deteriorated section of bridge deck (data courtesy of Ken Maser, Infrasense, Inc.)

One other effect that deserves mention is the delay in time of reflections from steel reinforcement. This is observed when the dielectric constant increases and causes a decrease in velocity of the EM waves (see Equation 2.3). If this is the case, and the conductivity is not high enough to completely attenuate the signal, the reflection will appear later in time. A section of bridge deck data exhibiting this, along

with various levels of attenuation, is shown in Figure 2.7. Interpretation of this effect is difficult because delay can be caused either by an increased dielectric constant in deteriorated concrete or by greater depth in sound concrete. Some variation in the thickness of the concrete cover layer due to inconsistencies in construction is a common occurrence (Maser K. R., 1996). This issue has been reported by multiple authors such as Sbartai et al. (2006) and a solution has been proposed by Barnes et al. (2008).

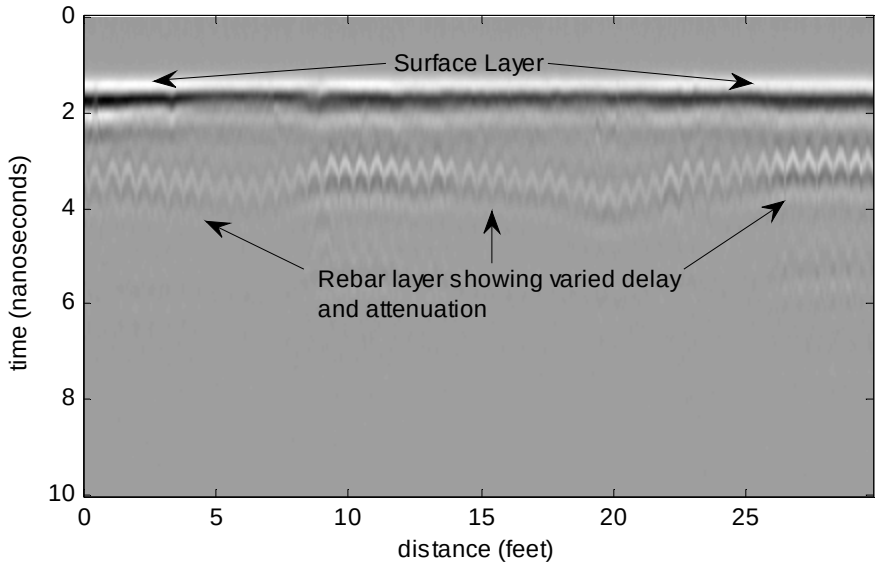

Figure 2.7: B-scan showing rebar layer with obvious variations (data courtesy of Ken Maser, Infrasense, Inc.)

2.3.3 Assessing the Accuracy of GPR Bridge Deck Investigations

Ground penetrating radar has been used to evaluate the condition of bridge decks starting in the early 1980s, and, since then, several studies have aimed to evaluate the overall accuracy of the technology and methods. The difficulty with such studies is that, to gain insight on the performance of GPR, the surface of the deck in question must be removed or the deck must be evaluated with a survey method that establishes ground truth. These methods include chain drag, half cell potential, and coring—all of which are cumbersome, expensive, and time consuming. Despite this, a number of studies have been

undertaken and generally good results using GPR to help make bridge deck repair decisions are reported (Maser, 1991; Maser & Rawson, 1992; Romero, G. E. Roberts, & R.L. Roberts, 2000).

In one pragmatic report, Barnes and Trottier (2000) perform surveys using high speed air coupled GPR antennas on a number of bridge decks. Of the surveyed decks, a small number are selected for repair and, prior to construction, are investigated with chain drag and half cell potential methods to obtain ground truth data. The success of GPR can be judged on two fronts. One is the spatial accuracy of identified deterioration, and the other is the overall quantity (surface area) of deteriorated deck. Identifying the location of deterioration is important to the repair process, while knowledge of the quantity of repairs required allows for accurate construction estimates and schedules as well as long term budget planning. The authors report that GPR was very accurate in predicting the actual repair quantities, with an average underestimate of 1.5%. This proved to be a significant upgrade over estimates made by visual inspection alone. However, the spatial accuracy proved less impressive, with GPR correctly predicting areas of deterioration 66.2% of the time and areas of sound concrete 77% of the time (both relative to a chain drag survey). The reason for the excellent quantitative predictions and only good spatial predictions is that the false positive and false negative predictions tended to cancel each other out. In other words, the number of times GPR erroneously reported deterioration roughly equaled the number of times GPR erroneously reported that the concrete was sound.

Barnes and Trottier (2002, 2004) also examine some of the phenomena responsible for incorrect predictions by GPR. As previously mentioned, the contrast between areas of sound and deteriorated concrete in a given deck plays a big role. Decks that have either low or high overall levels of deterioration are likely to exhibit this lack of contrast, making it difficult to achieve accurate results with GPR. The authors note that these decks are among the easiest to evaluate with a visual inspection, and suggest that a tandem of GPR and visual inspections could provide useful results. Since detection of

damage relies on the correlation between corrosion and high levels of moisture and chloride, any condition that alters this correlation can lead to errors. For instance, GPR may give different results depending on how dry or wet the weather has been preceding the survey (Barnes & Trottier, 2002). Rainfall will increase the moisture content in the deteriorated portions of the deck. Since GPR often relies on the presence of moisture to identify an increase in dielectric constant, lack of moisture in deteriorated areas may dim the contrast and make accurate detection of damage more difficult. For this reason, Barnes and Trottier (2002) suggest the best time to perform a GPR survey is after the surface has dried following a recent rainfall. Other factors that can significantly affect the GPR response are the condition of the asphalt overlay, variations in the depth of the reinforcement, and epoxy coatings on the reinforcement. In spite of these difficulties, the authors express optimism that with better understanding of the conditions that lead to false GPR predictions, detection algorithms can be advanced to give more accurate results.

2.4 Bridge Deck Investigations Using Computational Modeling

This study makes extensive use of a software package written by Dr. Kimberly Belli designed to model physical environments and simulate GPR responses in a computational environment. The software, known as an Integrated Sensor and Media Modeling Environment (ISMME), is described in detail by Belli (2008) and is briefly reviewed here. The ISSME is based in MATLAB and brings together two important pieces. The first is a well known method for simulating the propagation of EM waves, known as the Finite Difference Time Domain (FDTD) algorithm. The second is the ability to easily construct realistic models relevant to civil engineering in which EM waves are able to propagate.

2.4.1 Electromagnetic Wave Simulation in Two Dimensions with the Finite Difference Time Domain Method

The FDTD method is a popular way to simulate the behavior of EM waves because the method is fairly straight forward to implement and provides robust solutions to Maxwell's Equations. The method works by approximating the spatial and temporal derivatives of the electric and magnetic fields using a finite difference scheme.

In this simplified derivation, Maxwell's Equations are given in differential form by:

$$\nabla \times \boldsymbol{E} = -\mu \frac{\partial \boldsymbol{H}}{\partial t}$$
$$\nabla \times \boldsymbol{H} = \sigma \boldsymbol{E} + \epsilon \frac{\partial \boldsymbol{E}}{\partial t} \qquad 2.6$$

where $\boldsymbol{E}$ is the electric field, $\boldsymbol{H}$ is the magnetic field, t is time, μ is the magnetic permeability, and ϵ is the permittivity (Sadiku, 2001). Vector quantities are indicated in **bold**. Equation 2.6 is a set of vector equations that can be written as a system of six scalar equations. Before writing the scalar equations, it is noted that the software works with 2D geometries, with waves propagating in the $x - y$ plane. This is known as Transverse Magnetic mode (TM_z), where all partial derivatives with respect to z are zero. The only nonzero fields are expressed by $\{E_z, H_x, H_y\} \neq 0$. This simplification to 2D results in three scalar equations (Equation 2.7):

$$\frac{\partial H_x}{\partial t} = -\frac{1}{\mu}\frac{\partial E_z}{\partial y}$$

$$\frac{\partial H_y}{\partial t} = \frac{1}{\mu}\frac{\partial E_z}{\partial x} \qquad 2.7$$

$$\frac{\partial E_z}{\partial t} = \frac{1}{\epsilon}\left(\frac{\partial H_y}{\partial x} - \frac{\partial H_x}{\partial y} - \sigma E_z\right)$$

The nonzero fields are arranged in a grid pattern, shown in Figure 2.8, that offsets the field values by half a grid space ($\frac{\Delta x}{2}$ or $\frac{\Delta y}{2}$). This offset is the key to the FDTD algorithm, with each node in the grid containing the E_z field and each midway point between nodes containing either the H_x or H_y field. Time progresses in half step intervals and at each half or whole time step, only one of the fields ($\boldsymbol{E}$ or $\boldsymbol{H}$) is calculated. For example, at each whole time step the current electric field is calculated at each location in the domain from the surrounding magnetic field values and the previous electric field value at that location. At the next half time step, the roles are reversed and new magnetic field values are calculated from surrounding electric field values and previous magnetic field values. In this way, the algorithm steps forward in time while keeping track of fluctuations in the electric and magnetic fields.

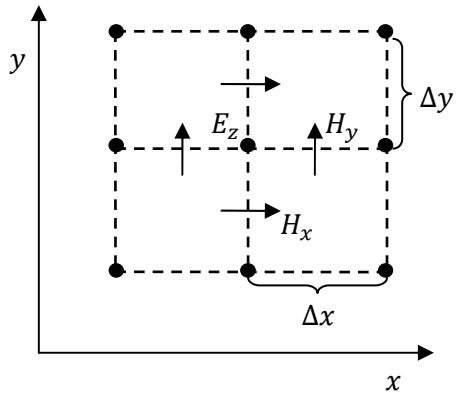

Figure 2.8: Arrangement of the electric and magnetic fields used in Equation 2.7

The FDTD algorithm is driven by the relationship between the magnetic and electric fields (Equation 2.7)—knowledge of each field is used to update the other. For these equations to be used in a time

stepping algorithm, the partial derivatives in Equation 2.7 must be approximated numerically. The method of approximation used is called a Finite Difference (FD) scheme and uses values of a function surrounding a point of interest to approximate the derivative at that point. Consider the function $f(x)$, and a point of interest x_0, where one wishes to evaluate the derivative. Using the central difference formula (one of the variations of the FD method) the derivative is approximated as

$$f'(x_0) = \frac{f(x_0 + \Delta x) - f(x_0 - \Delta x)}{2\Delta x} \qquad 2.8$$

Intuitively, the central difference formula (Equation 2.8) finds the slope between the points before and after x_0. A more general derivation with error considerations can be performed using a Taylor Series expansion and is presented by Sadiku (2001). The central difference variation is chosen for use in the ISSME software because the error is the smallest (Belli, 2008).

Since Equation 2.7 features derivatives with respect to both space and time, an indexing system of the following form is used where a function of two spatial dimensions and one temporal dimension is represented as

$$F^n_{(i,j)} \equiv F(i\Delta x, j\Delta y, n\Delta t) \qquad 2.9$$

The central difference formula is applied to the partial derivatives in Equation 2.10. Note that Equation 2.8 is general and can be used for a derivative with respect to space or time. In addition, the spacing between field values is half a grid space, so the 2 in the denominator of Equation 2.8 cancels out. For the ISSME implementation, it is assumed that material properties change as a function of location (Belli, 2008).

$$\frac{H_{x\,(i,j+1/2)}^{n+1/2} - H_{x\,(i,j+1/2)}^{n-1/2}}{\Delta t} = -\frac{1}{\mu_{(i,j+1/2)}} \frac{E_{z(i,j+1)}^{n} - E_{z(i,j)}^{n}}{\Delta y}$$

$$\frac{H_{y\,(i+1/2,j)}^{n+1/2} - H_{y\,(i+1/2,j)}^{n-1/2}}{\Delta t} = \frac{1}{\mu_{(i+1/2,j)}} \frac{E_{z(i+1,j)}^{n} - E_{z(i,j)}^{n}}{\Delta x}$$

2.10

$$\frac{E_{z(i,j)}^{n+1} - E_{z(i,j)}^{n}}{\Delta t} = \frac{1}{\epsilon_{(i,j)}} \left(\frac{H_{y\,(i+1/2,j)}^{n+1/2} - H_{y\,(i-1/2,j)}^{n+1/2}}{\Delta x} - \frac{H_{x\,(i,j+1/2)}^{n+1/2} - H_{x\,(i,j-1/2)}^{n+1/2}}{\Delta y} \right) + \sigma_{(i,j)} \left(\frac{E_{z(i,j)}^{n+1} + E_{z(i,j)}^{n}}{2} \right)$$

At this point, the bulk of the work is done and all that remains is to solve each expression in Equation 2.10 for the future field value, that is, field values with a time index of $n+1$ or $n+1/2$. Assuming a uniform grid and setting $\Delta x = \Delta y = \delta$, this yields the field update equations, which are listed in Equation 2.11.

$$H_{x\,(i,j+1/2)}^{n+1/2} = -\frac{\Delta t}{\mu_{(i,j+1/2)}\delta} \left(E_{z(i,j+1)}^{n} - E_{z(i,j)}^{n} \right) + H_{x\,(i,j+1/2)}^{n-1/2}$$

$$H_{y\,(i+1/2,j)}^{n+1/2} = \frac{\Delta t}{\mu_{(i+1/2,j)}\delta} \left(E_{z(i+1,j)}^{n} - E_{z(i,j)}^{n} \right) + H_{y\,(i+1/2,j)}^{n-1/2}$$

$$E_{z(i,j)}^{n+1} = \left(\frac{2\epsilon_{(i,j)} - \sigma_{(i,j)}\Delta t}{2\epsilon_{(i,j)} + \sigma_{(i,j)}\Delta t} \right) E_{z(i,j)}^{n} + \frac{2\Delta t}{\delta(2\epsilon_{(i,j)} + \sigma_{(i,j)}\Delta t)} \left[H_{y\,(i+1/2,j)}^{n+1/2} - H_{y\,(i-1/2,j)}^{n+1/2} + H_{x\,(i,j-1/2)}^{n+1/2} - H_{x\,(i,j+1/2)}^{n+1/2} \right]$$

2.11

Equation 2.11 constitutes the FDTD formulation of Maxwell's equations in the TM_z mode. Inspection of these equations makes clear that during half time steps, the magnetic fields are updated from existing values. During whole time steps, the electric field is updated from existing values. The alternate updating of the fields drives simulated EM wave propagation within the computational domain. A more

detailed derivation of the FDTD method including stability and boundary considerations as they relate to the ISSME is given by Belli (2008) and the FDTD method in 3D is derived by Sadiku (2001).

2.4.2 Physical Modeling

The physical modeling tool included with ISSME is designed to model physical environments and translate them to a numerical representation that can be used with FDTD simulation. The tool is designed with the modeling of civil infrastructure such as bridge decks and roadways in mind, though it can easily be extended to model any environment. To create a model, three steps are taken (Belli, 2008):

1) Create a 3D computational volume (called a scene)
2) Place relevant objects into the scene. These could include a concrete bridge deck, steel reinforcing bars, or a layer of asphalt. At this point, the material properties of the objects inserted into the scene have been defined.
3) Discretize the 3D volume into a 2D mesh, or slice, that the FDTD algorithm can work in. The resolution at which the scene is discretized can be adjusted based on the detail required. The 2D slice is a matrix whose entries contain the material properties at each location in space, among other information.

Since the model is in 2D there are some basic geometrical limitations. For instance, if a rebar is running in the longitudinal direction in the 3D scene, slicing through it to create the 2D model will result in the rebar appearing as a rectangular layer of steel. This layer of perfectly conducting material will completely obscure any objects beneath it. For this reason, rebar in this thesis is only modeled in the direction perpendicular to the slice.

Chapter 3: Antenna Characterization

Before meaningful simulations can be run with the ISSME software, the differences between a modeled 2D environment and the real 3D environment it represents must be taken into account. In 2D, waves propagate away from a point source in circles whose amplitudes are proportional to the inverse of the square root of the distance traveled from the source $\left(\approx \frac{1}{\sqrt{r}}\right)$. Circular waves in 2D would be represented by cylindrical waves in 3D. A point source in 3D produces spherical waves with amplitudes proportional to the inverse of the distance traveled from the source $\left(\approx \frac{1}{r}\right)$. This means that with a point source excitation, the reflection recorded in the 2D simulation will have a different amplitude than a reflection recorded in the analogous 3D scenario.

Ultimately, the goal is to be able to run simulations in 2D that have relevance to the 3D problem. One way to address this is by carefully choosing the excitation signal fed to the 2D FDTD simulation algorithm. Using a deconvolution method, the excitation signal can be configured to a reference case so that the desired 3D output results from the 2D simulation for that case. This method does not take into account the differences in propagation between 2D and 3D, and thus only works precisely in the reference scenario. Over the small distances generally encountered in bridge decks, this effect will slightly alter reflection amplitudes at depths not consistent with the reference, but the reflection shapes will remain accurate.

3.1 Theory

The excitation filtering process revolves around three relationships of the input-system-output variety, which are outlined in Figure 3.1. First, a reference system is chosen and a GPR antenna is used to collect the 3D response, preferably in a controlled environment. In this relationship, the input is the unknown excitation from the antenna, $x_a(t)$, the system is the reference system, $h_{3D}(t)$, and the output is the time history data collected by the GPR receiver, $y_{3D}(t)$.

The second relationship falls under normal operating procedures for running simulations with the ISSME software. Some excitation, $x(t)$, is fed into a 2D FDTD model of the reference system, $h_{2D}(t)$ (Figure 3.5 right), and produces simulated output, $y_{2D}(t)$. The third relationship is the desired scenario, where a configured excitation, $x'(t)$, is fed into the 2D FDTD model of the reference system, $h_{2D}(t)$, and the simulated output is the same as what was recorded by the GPR antenna for that reference case, $y_{3D}(t)$.

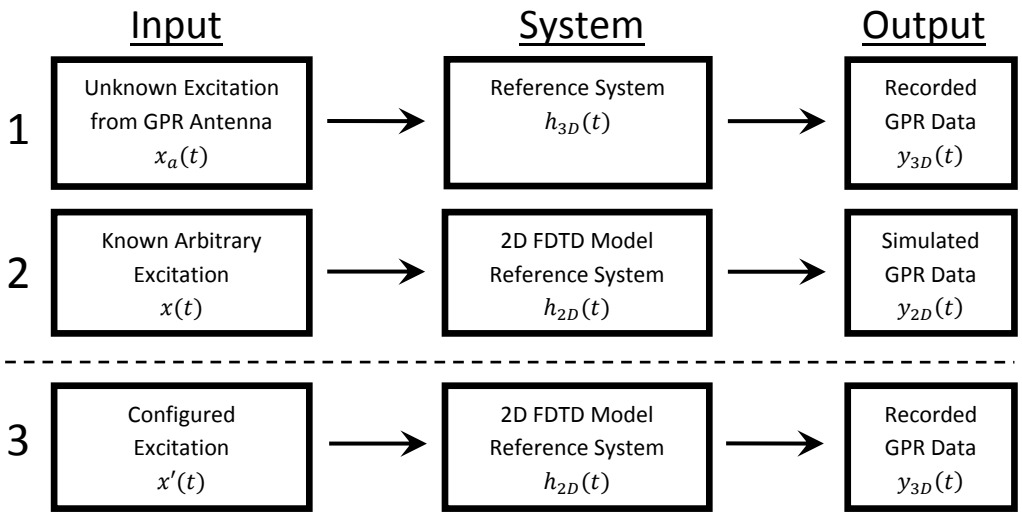

Figure 3.1: Diagram of the three input-system-output relationships used to configure the FDTD excitation

When viewed in the time domain, the relationship between the inputs, systems, and outputs is a convolution where the input is difficult to solve for because it exists under an integral. Using the well known Fourier Transform, $\mathcal{F}[g(t)] = G(f)$, the relationships are expressed as functions of frequency, f. One effect of this transformation is that integration in the time domain becomes multiplication in the frequency domain, making it easier to solve for the desired input. The valid equations in the frequency domain are shown in Equation 3.1.

$$X_a(f)H_{3D}(f) = Y_{3D}(f)$$

$$X(f)H_{2D}(f) = Y_{2D}(f) \qquad 3.1$$

$$X'(f)H_{2D}(f) = Y_{3D}(f)$$

From the second expression in Equation 3.1, the relationship $H_{2D}(f) = Y_{2D}(f)/X(f)$ can be derived. When substituted into the third expression, the configured excitation $X'(f)$ can be solved for (Equation 3.2).

$$X'(f) = \frac{Y_{3D}(f)}{Y_{2D}(f)}X(f) \qquad 3.2$$

The inverse Fourier Transform, $x'(t) = \mathcal{F}^{-1}[X'(f)]$, is used to bring the configured excitation signal back to the time domain where it can be used with the 2D FDTD model.

3.2 Metal Plate as a Reference Case

Initial efforts to calculate a configured excitation employed metal plates buried in sand as the reference cases. Three plates allowed for investigation of how depth affected the received signal and configured excitation and made it easy to calculate the dielectric constant of the sand for modeling purposes. The three plates, each roughly 24” long and 18” wide, were buried at depths of 6”, 9”, and 12”. Plexiglas sheets were placed on the surface of the sand to allow the antenna to roll while collecting data. This setup and the 2D FDTD model of it comprise three separate reference cases ($h_{3D}(t)$ and $h_{2D}(t)$ for each of the three plates) and are shown in Figure 3.2.

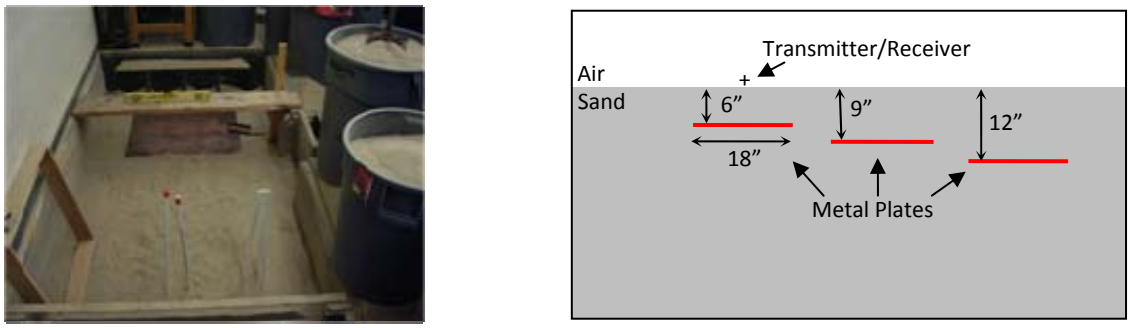

Figure 3.2: *Left:* Burying the deepest of 3 metal plates for the reference system. *Right:* 2D FDTD model of the reference system

A 1.5GHz ground coupled antenna is used to collect a B-scan (Figure 3.3 left) over the sand bed and three scans (time histories) taken from above each plate are used as separate measurements of $y_{3D}(t)$, one for each of the reference cases. Scans with a minimal amount of secondary reflections and noise were chosen for this purpose. Since the goal is to accurately simulate the target reflection, rather than the entire scan, these three scans are cleaned by time gating the signal to include the metal plate reflection only (Figure 3.3 right). Each is then used to calculate one of three configured excitations using Equation 3.2: $x_6'(t)$, $x_9'(t)$, and $x_{12}'(t)$. The excitations are calculated using three different simulated scans of $y_{2D}(t)$, each obtained by placing the transmitter and receiver over one of the three metal plates in the model.

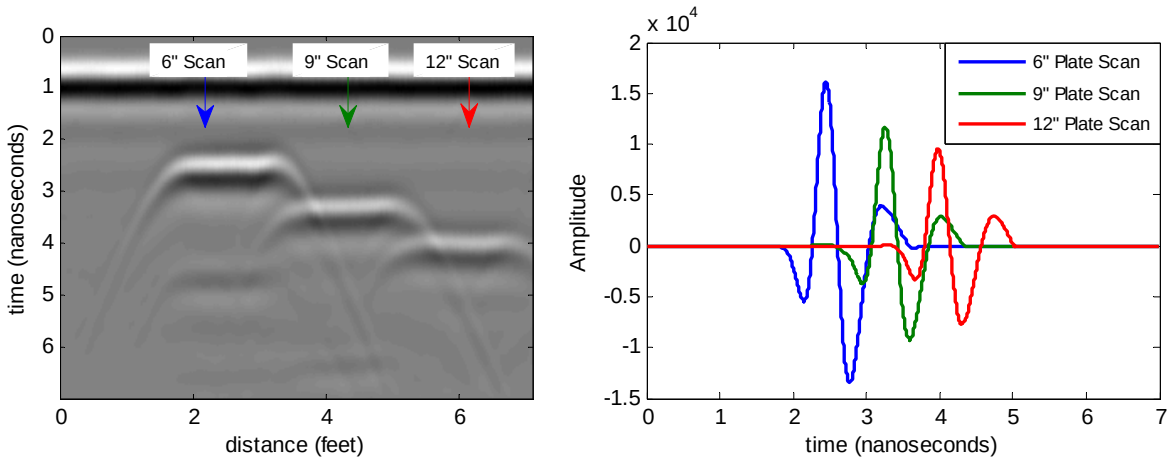

Figure 3.3: *Left:* B-scan showing reflections from 3 metal plates and locations of scans (time histories) for each plate. *Right:* Cleaned scans for each plate showing only the metal plate reflections

Figure 3.4 shows a comparison between 3D reference scans and 2D simulations using $x_6'(t)$ as the configured excitation. Again, the focus is on the metal plate reflections, so the remainder of each scan is removed by time gating. The reference scan for the 6" plate and the simulation for the 6" plate match precisely by definition—$x_6'(t)$ was calculated so that it would produce the same metal plate reflection as seen in the reference scan. When $x_6'(t)$ is used to collect a simulated scan over the 9" plate, one observes that the amplitude is slightly higher than the reference scan for the 9" plate. This is because waves decay more quickly propagating in 3D than they do in 2D. If a gain were applied to the 2D scans as a function of the distance to the source of the wave (r), the amplitude would match the 3D data and the shape of the wave would remain an excellent match. To complete the analysis, if simulations over each plate were run using $x_9'(t)$ as an excitation, the 2D scan over the 9" plate would match the 3D 9" reference scan precisely while scans over the other two plates would match in shape but would differ in amplitude compared to the respective 3D references.

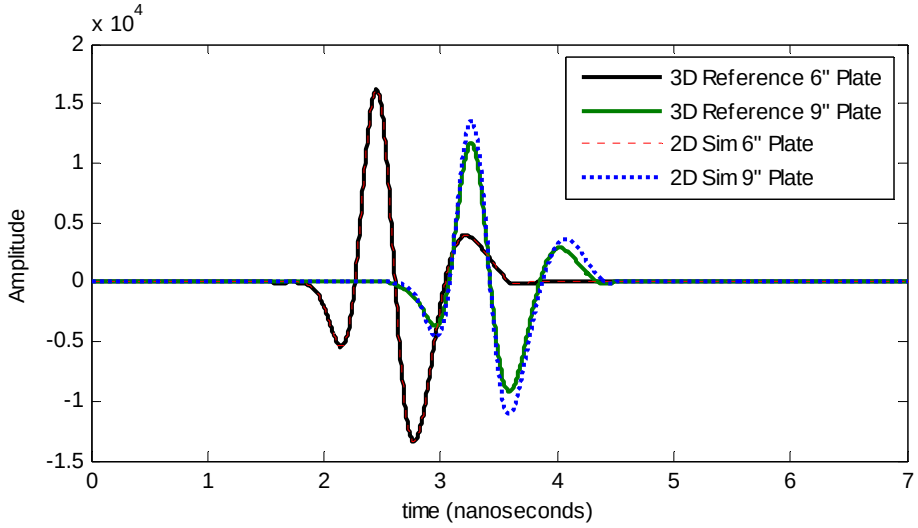

Figure 3.4: Comparison of 3D reference scans and 2D simulated scans using $x_6'(t)$ as an excitation signal.

3.3 Rebar as a Reference Case

Since the primary target of simulations in this work is rebar, the configuration process was repeated using a single rebar as the reference case. The desired 3D output for the reference case was determined by burying a section of 5/8" diameter rebar in sand and collecting data using a ground coupled GPR antenna (Figure 3.5 left). The rebar was buried 9" deep to ensure its reflection was completely separate from the surface reflection (this is necessary to allow for the removal of the surface reflection prior to the filtering process). The corresponding 2D FDTD model is shown in Figure 3.5 right.

Figure 3.5: ***Left:*** **Collecting GPR data for the reference case.** ***Right:*** **2D FDTD model of the reference case**

The configured and arbitrary normalized excitations ($x'(t)$ and $x(t)$) are shown in Figure 3.6 left. The response when $x'(t)$ is used with the 2D reference model is shown in Figure 3.6 right alongside the GPR response to the 3D reference model for comparison. The plot shows that, as expected, the rebar reflection is nearly identical in both cases. The surface reflections are different because they are removed from y_{2D} and y_{3D} prior to the configuration process. The surface reflection in the GPR data depends on the physical configuration of the antenna and the materials used in the antenna housing. These parameters are difficult to determine, and since the focus is on the rebar reflection, they were left out of the model.

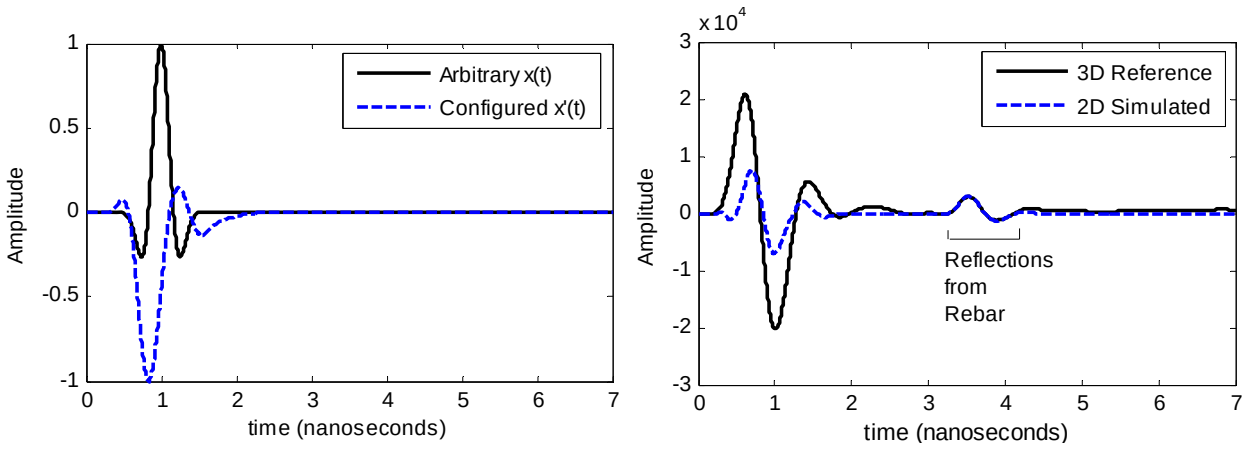

Figure 3.6: *Left:* Normalized excitations used with the 2D FDTD model. *Right:* Comparison of reference case GPR data to simulated response using the configured excitation

The configured excitation in Figure 3.6 was used for the remainder of the simulations reported in this thesis. The amplitude of the rebar reflection using this excitation will only match the 3D case when the rebar is at the same depth as in the reference case. However, the shape will be consistent at all depths and the difference in magnitude can be easily corrected by applying a gain if a direct quantitative comparison between simulated and real data is desired. For this investigation, qualitative comparisons are made between real and simulated data, while quantitative comparisons are made only between simulated data sets.

Chapter 4: Modeling Deterioration

Mixture models strive to describe the final material properties of a conglomerate composed of several ingredient materials whose properties are known. This technique can take a number of theoretical approaches and several of these that are applicable to concrete are described by Halabe (1990). The models examined here differ from mixture models in several ways and one is that they are not formulated analytically. Rather, a data driven approach is taken where data signatures that are generally

thought to represent deterioration are analyzed to determine the conditions in the bridge deck that could have caused them. These signatures are described in detail in Section 2.3.2 and are characterized by increased delay and attenuation of the rebar reflection and increased amplitude of the surface reflection.

The causes for these detectable changes in the material properties of concrete come from cracking that emanates from the steel reinforcement and contaminants that penetrate from the surface. Since both processes occur gradually and have clear sources of origin, there is reason to believe that the changes in material properties that correlate to deterioration may vary in magnitude within the concrete. While it is likely that at some stage in the deterioration process the concrete takes on more or less uniform material properties, particularly in the cover layer, it is reasonable to suggest that these changes begin as gradients extending from their respective sources. Understanding how GPR responses are affected by these gradients in material properties plays a big part in correlating radar signatures with real bridge deck conditions.

Traditional mixture models have successfully combined aggregates, cement, water, and chlorides to arrive at specific material property values. In the material models investigated here (which are not mixture models in the traditional sense), the emphasis is less on specific values and more on how changes relative to sound concrete are distributed through the slab. For this reason, the models here should be viewed qualitatively with the understanding that a range of specific values could be applied under the proposed distributions. To be clear, the purpose is to investigate conditions in the bridge deck that are reasonable in a physical context and that produce GPR responses often correlated with corrosion—not to validate the modeling tools.

Dielectric constant and conductivity play the prominent roles in terms of how GPR waves behave in concrete. It is assumed here that the GPR frequency is confined to a limited range and that these

properties do not vary within that frequency range. In addition, it is assumed that the two properties have some conditional dependence on each other. For instance, the presence of moisture may result in a large change in the dielectric constant while the conductivity is only slightly altered from that of dry concrete. A large change in conductivity is associated with the presence of chloride ions, but only if they are in solution. Therefore, high conductivity and a dielectric constant that remains unchanged is not a likely scenario. In general, an increased dielectric constant is responsible for delay of reflections and conductivity for their attenuation. Since both effects are observed in radar data, and since increased conductivity implies the presence of moisture, gradients for both properties are defined over the same spatial range.

First, this section describes an experiment that justified the exploration of gradients of material properties. Next, a 2D FDTD bridge deck model is developed and two models for changes in material properties are proposed and investigated. Lastly, the results of a parameter study are presented that describe how changes in specific parameters of one model can affect the GPR response.

4.1 Experiment: Altering Material Properties Surrounding Reinforcement

An experiment was performed to assess how altering material properties in the vicinity of steel reinforcement would affect the GPR response.

4.1.1 Experimental Setup

Each sample was buried in dry sand in a controlled environment. The test setup consisted of #5 rebar (5/8” diameter) seated in the center of a 1.5” diameter PVC pipe using plastic spacers at each end (Figure 4.1 left).

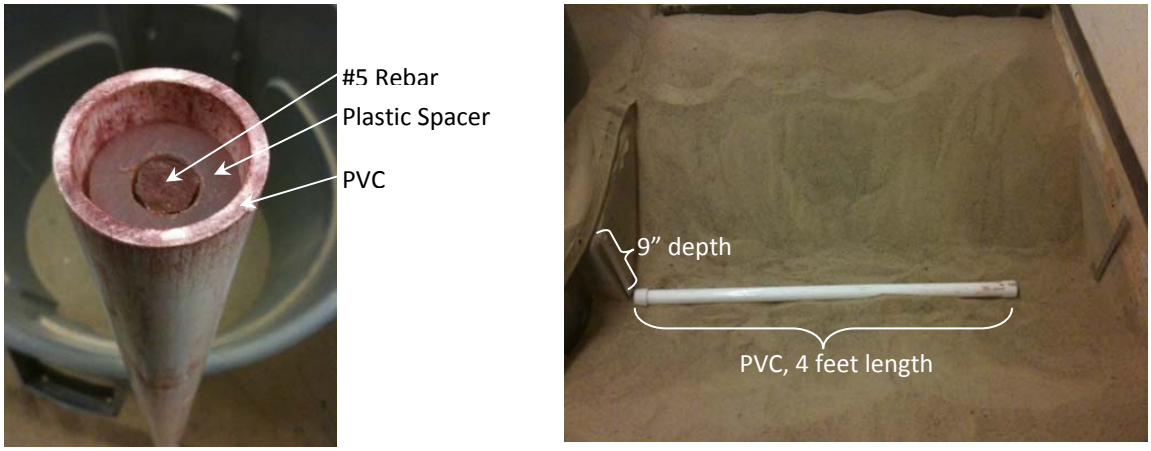

Figure 4.1: *Left:* Experimental setup with PVC, spacer, and rebar. *Right:* PVC placed in soil bed prior to burying

For each sample, the remaining volume inside the PVC pipe was filled with one of three test mixtures: dry sand (reference), sand saturated with water, and sand saturated with salt water. These test mixtures were designed to simulate contaminated material that may surround corroding rebar. The mixtures were packed into the PVC pipe to eliminate air voids and the ends were capped before burying the entire mixture, rebar, and PVC combination 9 inches deep in sand (Figure 4.1 right). In an additional test case, the rebar was left out and the PVC was filled only with dry sand. This was to show that the PVC had no noticeable effect on the GPR response (PVC has a dielectric constant very near that of dry sand).

Data were collected using a GSSI 1.5 GHz ground coupled antenna. After each test case was buried, thin plexi-glass sheeting was used to cover the surface of the sand to allow the antenna to roll. The antenna was passed down the centerline of the soil bed to minimize interference from the sides of the bed.

4.1.2 Case 1: PVC and Dry Sand

When the PVC pipe was filled only with dry sand, the B-scan (Figure 4.2) showed no indication of a buried target. This is because the difference in material properties between sand and PVC is not big enough to cause a reflection. This confirms that the presence of the PVC does not alter the GPR response.

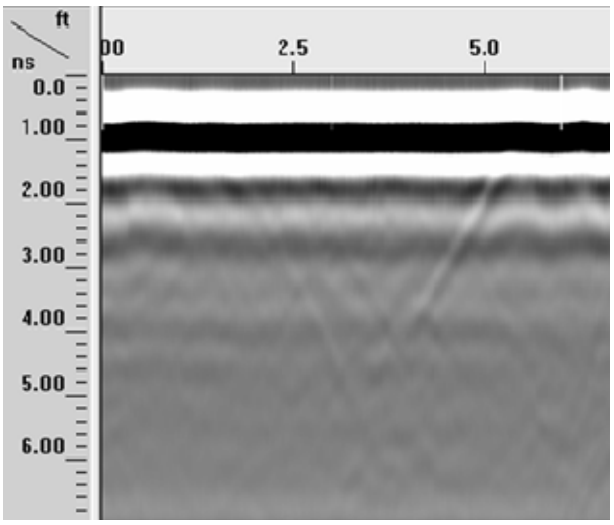

Figure 4.2: Case 1: B-scan of soil bed with PVC filled with dry sand shows no indication of the buried target

4.1.3 Case 2: PVC, Rebar, and Dry Sand (Reference)

The reference case represents healthy rebar surrounded by material free of contaminants or defects (analogous to sound concrete). The B-scan (Figure 4.3 left) shows a normal rebar reflection. This is expected given the results of case 1, which determined that the PVC has no discernable effect on the GPR response.

4.1.4 Case 3: PVC, Rebar, Saturated Sand

A portion of sand was saturated with tap water before being packed into the PVC pipe along with the rebar. Excess water that surfaced after packing was poured off. This case represents moisture that may be present in the material surrounding the rebar. The B-scan (Figure 4.3 center) shows 2 reflections. One is from the PVC-wet sand interface (the dry sand and PVC essentially act as one medium because of their similar properties). The other is from the rebar, which appears later in time compared to the rebar reflection in the reference case. This is because wet sand has a higher dielectric constant than dry sand and thus EM waves travel more slowly in the wet sand within the PVC pipe, leading to a slightly later arrival time of the rebar reflection.

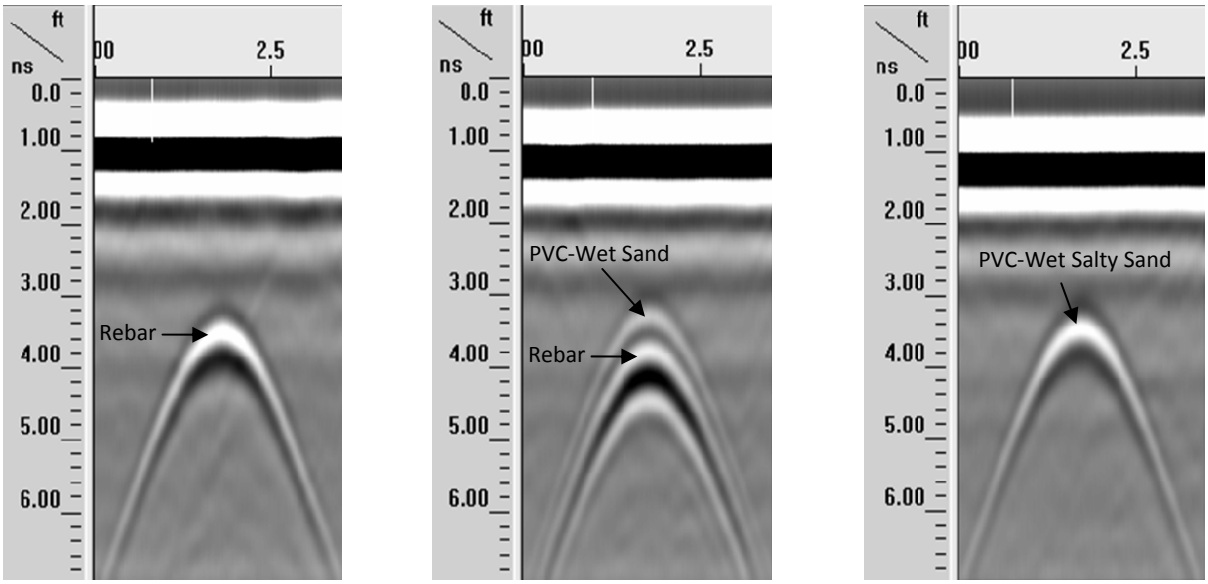

Case 2 (reference): PVC, Rebar, Dry Sand

Case 3: PVC, Rebar, Saturated Sand

Case 4: PVC, Rebar, Brine Saturated Sand

Figure 4.3: B-scan results for test cases 2, 3, and 4

4.1.5 Case 4: PVC, Rebar, Brine Saturated Sand

The same setup was used as in case 3, except that salt was first dissolved into the water before saturating the sand. This case represents rebar surrounded by material contaminated with both moisture and chlorides. The B-scan (Figure 4.3 right) shows one reflection from the PVC-wet, salty sand interface. With the addition of salt, the mixture inside the PVC pipe becomes highly conductive. Any signal that passes into this region is quickly attenuated and explains why no reflection from the rebar can be seen.

4.1.6 Conclusions

This experiment shows the GPR response when contaminants known to be present in bridge decks surround the rebar. Of note is the fact that the responses observed do not display the delay and attenuation of the rebar reflection generally associated with ingress of moisture and chloride. This leads one to believe that this experiment does not represent the real situation. The reason for this is the distinct interface between healthy and contaminated material. These sudden changes in material properties are responsible for the GPR responses observed and most likely do not occur in bridge decks.

A far more likely scenario is that the changes in material properties occur over some distance, resulting in gradients.

4.2 The 2D FDTD Bridge Deck Model

For the computational investigation, a simple model bridge deck was developed. The model has physical dimensions typical of a bridge deck. The slab is 7.25” thick and has #5 rebar (5/8” diameter) spaced at 8” intervals 2.75” beneath the deck surface. For simplicity, an asphalt overlay is not included. It is expected that inclusion of an overlay would not affect the overall conclusions of the investigation. Healthy concrete is modeled having a dielectric constant of 6.25 and 0 conductivity.

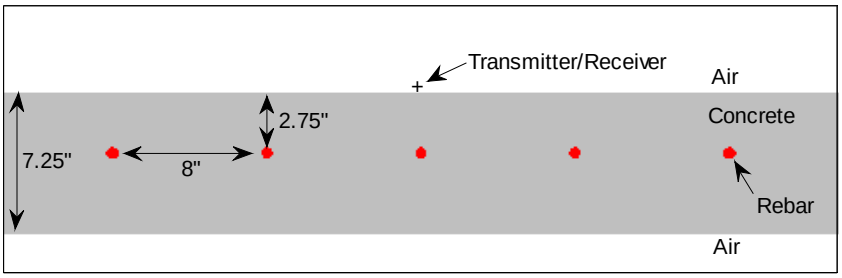

Figure 4.4: Bridge Deck Modeled with the ISSME software

The model, shown in Figure 4.4, is a 2D slice of the 3D scene. Since the ISSME was formulated in 2D, this discretization is necessary, and, if one assumes no physical changes in the third dimension, is adequate to represent the real 3D situation. The location of the transmitter and receiver is represented by the ‘+’ symbol. Each simulation will collect a scan from that location. To simulate a B-scan, the transmitter and receiver are moved from the left side of the model to the right, collecting scans at set intervals.

4.3 Model 1: Contamination Extending From the Reinforcement

This model represents a scenario that likely would occur after the corrosion process is underway. As the rebar expands, cracks extend from the rebar creating a localized area of very permeable concrete. When

contaminants penetrate from the surface, they may become trapped in the area surrounding the rebar. As previously mentioned, it is unlikely that GPR can reliably detect the cracks themselves, and therefore successful detection of corrosion will result from detecting contaminants trapped in these areas.

This material model (shown in Figure 4.5) represents a section of contaminated concrete within an otherwise sound bridge deck, with the worst contamination concentrated around the center rebar. The contaminated area extends horizontally and affects the adjacent rebar to a lesser extent. Profiles of the dielectric constant and conductivity through the center rebar are shown in Figure 4.6. The specific values in these profiles represent an example of material property values that are reasonable for contaminated concrete. Many other cases are possible where the maximum and slope of the gradient take different values. In this case it is assumed that changes to the material properties of the concrete extend a maximum of an inch from the rebar surface.

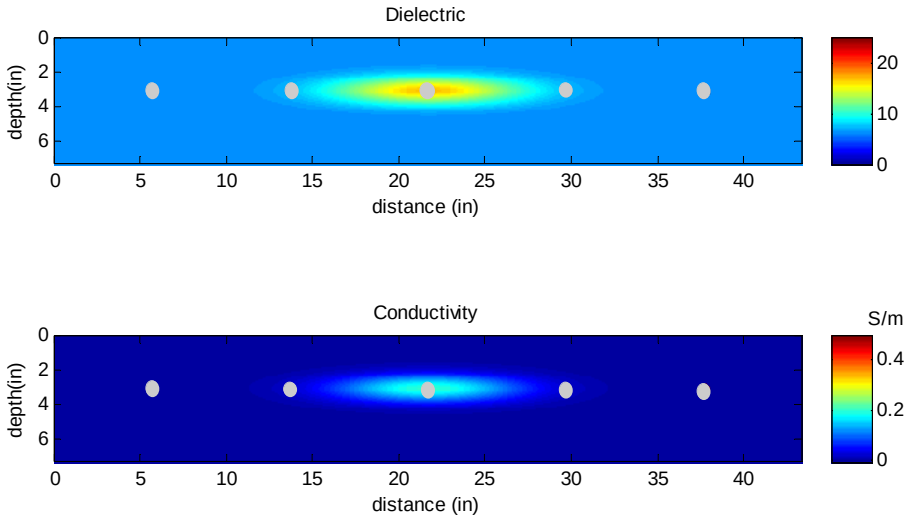

Figure 4.5: Mapping of dielectric and conductivity for Model 1 with contamination extending from rebar (gray)

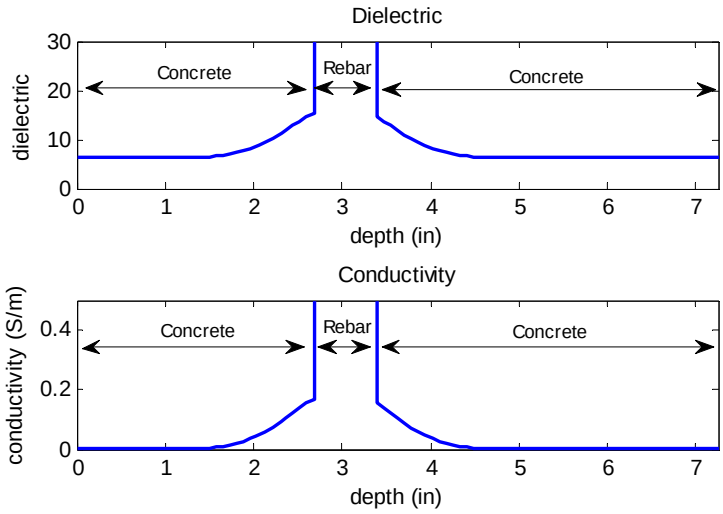

Figure 4.6: Profiles of material properties through the center rebar for Model 1

The GPR response to these conditions is shown in a simulated B-scan in Figure 4.7. The rebar reflection in the contaminated area has been delayed and attenuated. The amount of delay and attenuation could be changed in similar models by adjusting the parameters of the gradient; however, if the gradient is too steep, a reflection will appear from the gradient. In this example, there is some evidence of a reflection from the gradient just above the contaminated rebar reflection in Figure 4.7. If the gradient were to extend further toward the surface, the reflection from the gradient may combine with the surface reflection and become difficult to recognize as a distinct reflection. Since the surface is not affected in this model, there is no increased surface reflectivity in the contaminated region.

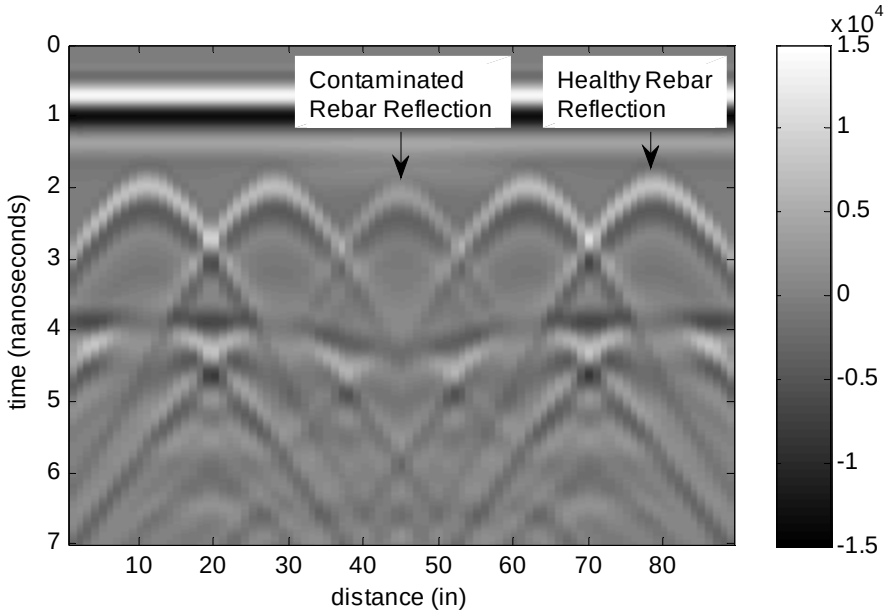

Figure 4.7: Simulated B-scan of Model 1 showing delay and attenuation of the rebar reflection in the contaminated area

To produce delay and attenuation of the rebar reflections, the parameters on the gradient in this case must be fairly strict. If the gradient is too steep, a reflection from the gradient will make this obvious, even if partially masked by proximity to the surface. Reflections from a gradient can be reduced by refining the discretization of the model so that the material property changes from pixel to pixel are smaller. However, these stipulations for smoothness and continuity of the gradient approach a level of detail and consistency that is not likely to be realistic. In light of this, it was concluded that the area surrounding the rebar must not be the only region affected by contaminants.

4.4 Model 2: Contaminants Concentrated Below the Surface

A material model where contaminants enter from the surface and become concentrated in the concrete layer above the rebar makes sense for several reasons. As rainfall or snowmelt saturate the surface, moisture will penetrate into the porous concrete medium, especially in areas of weak concrete. This moisture moves through the concrete slab slowly, and, if it comes into contact with the steel reinforcement, will eventually start the corrosion process. It is not common practice to perform GPR

surveys when the surface is wet and it is therefore unlikely that the surface itself will have high dielectric and conductivity. The more probable scenario is that moisture content begins to rise just under the surface and then reaches a maximum and falls off according to parameters involving the concrete porosity, health, and time and weather conditions since the surface was wet.

An example of what this model might look like is shown in Figure 4.8. Again, dielectric and conductivity gradients are correlated spatially because of the assumed dependence on moisture in increasing them beyond their nominal values. The contaminated area is concentrated above the center rebar and profiles of the properties at that location are shown in Figure 4.9. While the example uses specific values that are reasonable, it is presumed that many variations exist following similar qualitative logic. Parameters that could vary include the maximum value, proximity of the maximum to the surface, and rate with which the curves return to their nominal values.

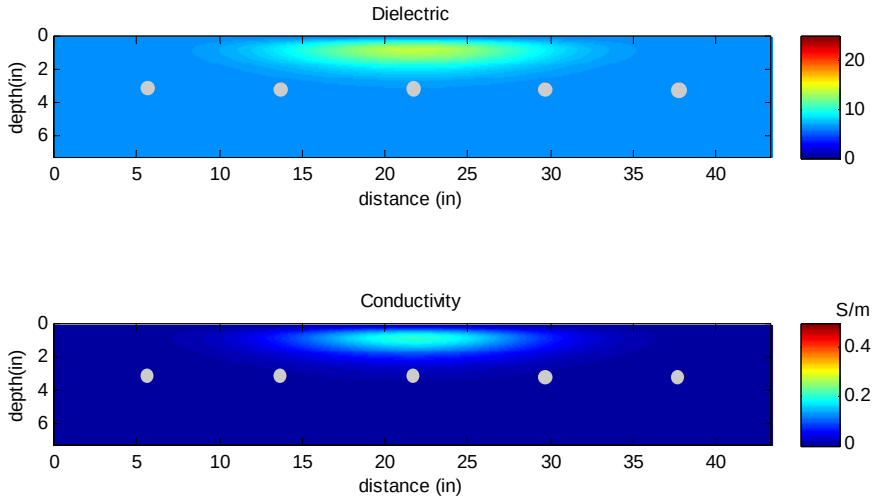

Figure 4.8: Mapping of dielectric and conductivity for Model 2 with contamination concentrated under the surface (rebar in gray)

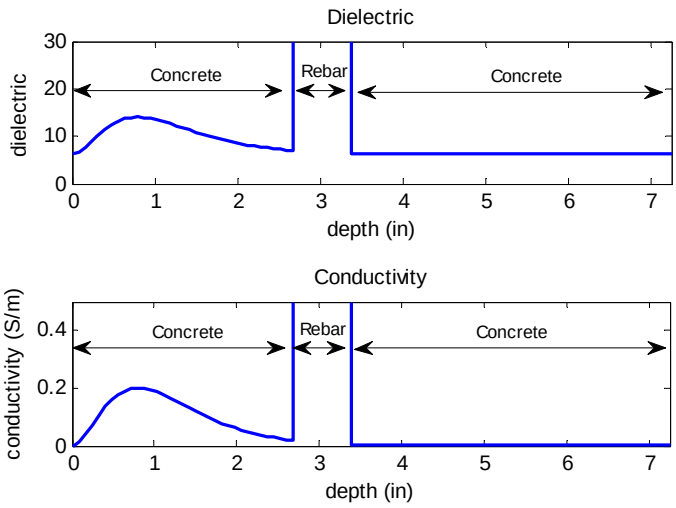

Figure 4.9: Profile of material properties through the center rebar in Model 2

Delay and attenuation of the rebar reflection are observed in the simulated B-scan (Figure 4.10) throughout the contaminated region of this model. There are also no reflections from the gradient in the contaminated region. The ascending gradient doesn't show up as a distinct reflection because it is too close to the surface and combines with the surface reflection. Depending on how close to the surface and how steep the gradient is, the surface reflection can be increased. The amount of increase ranges from significant to small enough that it could fall under normal variation for GPR data collected in the field. This suggests the practice of using increased surface reflectivity to diagnose contaminated regions of concrete may not be completely reliable and could explain why some areas of damage are missed.

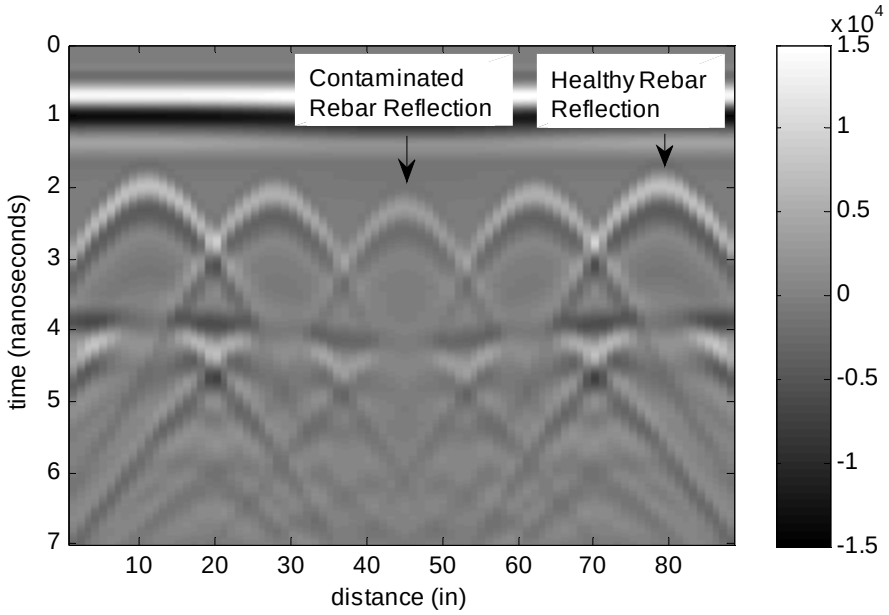

Figure 4.10: Simulated B-scan of Model 2 showing delay and attenuation of the rebar reflection in the contaminated area

No reflections are observed from the descending gradient because those small reflections are deflected back into the region of high conductivity that attenuates the reflections. The reflection from the rebar is strong enough to make it back to the receiver, but appears weak. It is noted that this attenuation is produced without contamination surrounding the rebar and may help to explain some of the false diagnoses of deterioration made by GPR.

In this scenario, neither the ascending nor descending gradients are required to be smooth to produce the effects observed in GPR bridge deck data. If Models 1 and 2 were combined so that contamination was present surrounding the rebar and in the layers covering the rebar, the gradient around the rebar would not have to be smooth because any small reflections would be attenuated by the layer of high conductivity above it. For these reasons, early stages of contamination are likely to resemble Model 2, while later stages of deterioration may be represented by a combination of the two models.

4.5 Parametric Study

Model 2 was selected for further exploration to examine how early stages of contamination might affect the GPR response. A parameter study was performed in which three sets of simulations were carried out. The main variation in the material model between simulations was the maximum value of the dielectric constant and conductivity.

The bridge deck model established in Section 4.2 was used and each simulation consisted of collecting one scan (time history) with the transmitter and receiver directly over the center rebar. The uniform reference condition was concrete with a dielectric constant of 6 and conductivity 0 S/m. In each set of ten simulations, the reference condition of the concrete was changed by introducing property gradients according to Model 2. The first simulation in each set is the reference condition. In subsequent simulations, the dielectric constant and or conductivity were increased incrementally to a maximum value. In the first set, the dielectric constant was increased from 6 to 30 while the conductivity was increased from 0 S/m to 0.4 S/m. This means that the second simulation in the set used a material model with a maximum dielectric constant of 8.67 and maximum conductivity of 0.044 S/m. In the second set the dielectric constant remained at the nominal value for all simulations while the conductivity was increased from 0 S/m to 0.4 S/m. In the third set the dielectric constant was varied between 6 and 30 while the conductivity was held constant at the nominal value.

The results of these simulations are helpful in determining how changes in the dielectric constant and conductivity affect the GPR response. Of primary interest are the delay and attenuation of the rebar reflection (from the rebar directly beneath the transmitter/receiver). Both of these quantities are measured relative to the nominal conditions. The delay is measured as the difference in peak arrival time of the rebar reflection compared to the peak arrival time in the reference case. If the attenuation was measured as a difference, the values would not translate from the 3D reference to the 2D

simulations. Instead, the attenuation is measured as a percent decrease in amplitude of the rebar reflection compared to the reference, which has the advantage of translating between 2D and 3D.

The delay and attenuation versus the maximum parameter on the material model for each simulation is shown in Figure 4.11. In the first case (blue) where both the dielectric constant and conductivity are changing, delay and attenuation of the rebar reflection were observed. In the second case (green), where the dielectric was held constant while the conductivity was varied, attenuation but no delay is observed. In the third case (red), the rebar reflection is delayed but not attenuated because the conductivity was held constant while the dielectric was varied. In each case the first data point represents the reference conditions, so there is neither delay nor attenuation.

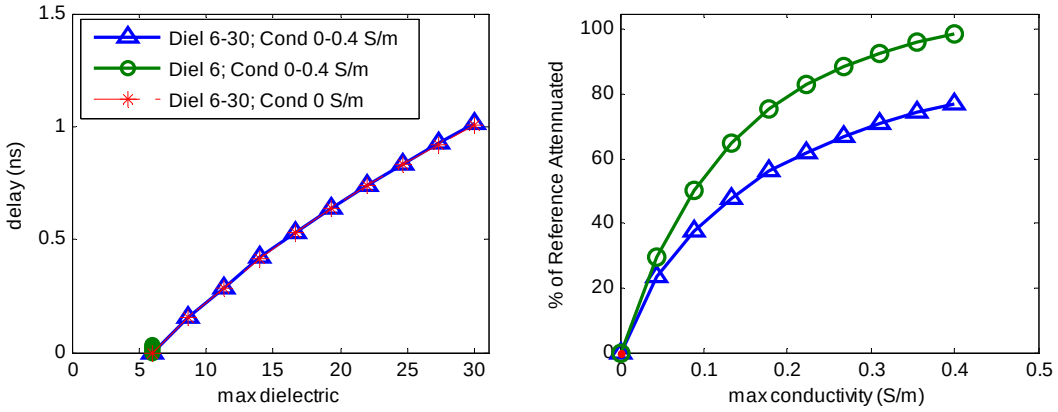

Figure 4.11: ***Left:*** **Delay of the rebar reflection vs. the maximum dielectric constant in the material model.** ***Right:*** **Attenuation of the rebar reflection vs. the maximum conductivity in the material model**

Figure 4.11 left shows that delay of the rebar reflection is solely dependent on the change in dielectric constant, which is expected due to the fact that delay is a direct consequence of decreased wave velocity (see Equation 2.3). In Figure 4.11 right, the divergent curves show that attenuation depends on both the dielectric constant and conductivity. When both properties are varied the attenuation is less

than if only the conductivity was increased. This result is predicted by the expression for the loss tangent: $\tan\delta = \frac{\sigma}{2\pi f\epsilon}$. That is, for given conductivity the loss decreases as the permittivity increases.

If the general parameters of material Model 2 are accepted, the change in dielectric constant and conductivity between sound and contaminated concrete can be estimated. As an example, two sections of GPR data taken from the same bridge deck were considered (Figure 4.12 left, center). One was chosen as a reference and exhibits characteristics of sound concrete: strong rebar reflections that occur early in time. The other shows indications of contamination, namely weak rebar reflections that occur late in time. In the following analysis the sound concrete is assumed to have a dielectric constant of 6 and conductivity of 0 S/m. Small errors in these assumptions will not significantly alter the calculated material property changes.

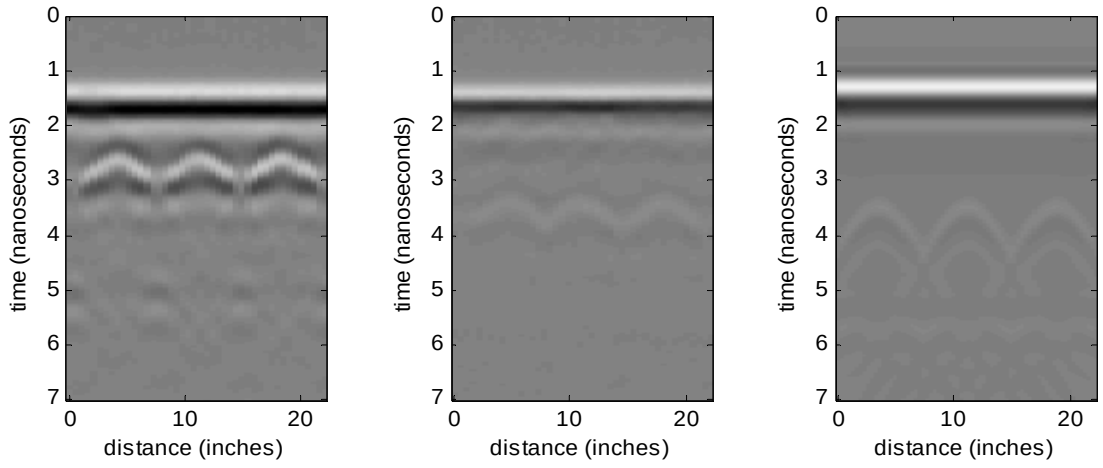

Figure 4.12: ***Left:*** **Reference GPR data.** ***Center:*** **Contaminated GPR data.** ***Right:*** **Simulated B-scan using material Model 2 and calculated parameters (GPR data courtesy of Ken Maser, Infrasense)**

By examining scans from each section of data (Figure 4.13), the delay and attenuation experienced by the rebar reflection in the contaminated section were determined to be 0.8 ns and 80% compared to the reference reflection. Referring to Figure 4.11 left, a delay of 0.8 ns corresponds to a dielectric constant of 23.6, or an increase of 17.6 compared to the reference. Due to the fact that attenuation

depends on both conductivity and dielectric constant, the change in conductivity cannot be similarly determined. A set of simulations were run keeping the maximum dielectric constant at 23.6 while increasing the conductivity from 0 S/m to 0.5 S/m. This set of simulations formed a plot (not shown) similar to Figure 4.11 right, which accurately describes the attenuation in the presence of increased dielectric constant. From this plot, the change in conductivity was determined to be 0.39 S/m. Investigations showed that as long as the actual reference conditions were reasonably close to the modeled reference conditions, the changes in material properties could be calculated without significant error. Discrepancies of up to 2 for the dielectric constant and 0.1 S/m for the conductivity were investigated in the assumed reference properties.

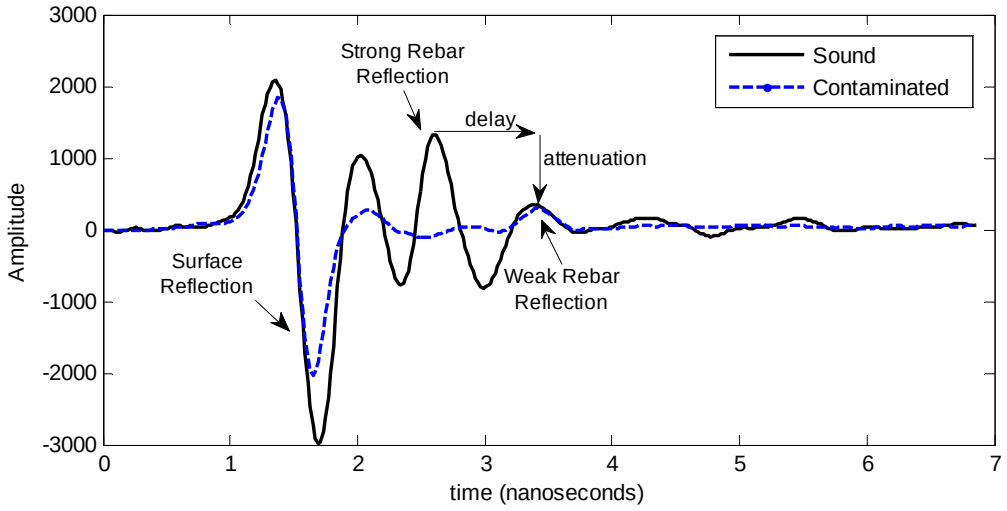

Figure 4.13: Comparison of center rebar scans where in contaminated concrete the rebar reflection is delayed and attenuated compared to the rebar reflection in sound concrete

The calculated changes in the dielectric constant and conductivity of the contaminated section of bridge deck data were used to create a material model of a contaminated bridge deck (Figure 4.14). The simulated B-scan for this model is shown in Figure 4.12 right and represents a close match to the contaminated GPR data.

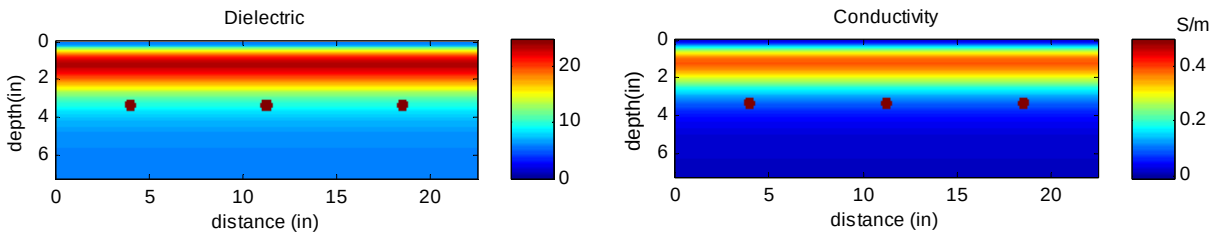

Figure 4.14: Material model for contaminated concrete with parameters calculated from GPR bridge deck data

Chapter 5: Summary and Conclusions

Indicators of bridge deck damage in GPR data, namely delay and attenuation of the rebar reflection, were successfully reproduced in simulated GPR responses using a modeled bridge deck. Variations from healthy bridge deck responses were produced by changing the material properties of the concrete deck slab. These changes fell into one of two categories and constituted two material models. In Model 1, changes in the material properties of the concrete extend from the rebar as a result of contaminants that may be caught in cracks close to the rebar. Gradients were employed such that the most drastic changes to the concrete were found next to the rebar and then decreased moving away from the rebar. Model 2 represented a situation where contaminants penetrate from the surface and become concentrated in the layers of concrete above the rebar. It was assumed that the surface was dry at the time of survey so that the most drastic change to the concrete was encountered below the surface. From the maximum, the changes to the concrete decreased with depth following the assumption that fewer contaminants are able to penetrate deeply into the concrete.

For both models, examples were presented where the simulated responses showed delay and attenuation of the rebar reflection. In Model 1, it was noted that smooth and generally shallow gradients were required to avoid producing reflections from the gradient. Because it is unlikely that

smooth gradients exist with regularity in bridge decks, it was concluded that this model by itself was unrealistic. Model 2 resulted in delay and attenuation of the rebar reflection without stipulations on the smoothness or slope of the gradient. This was because the area of relatively high conductivity near the surface attenuated any small reflections that resulted from steep or inconsistent gradients. It was concluded that Model 2 likely represented an early stage of deterioration when contaminants first begin to penetrate the concrete and that later stages of deterioration might be represented by a combination of Models 1 and 2.

It was emphasized that the goal of these models is to propose the qualitative distribution of contaminants in concrete rather than specific material property values. The dielectric constant and conductivity values used in the examples represent reasonable samples. The proposed models can be scaled within that range depending on the state of contamination one wishes to model. For Model 2, scaling of the model was investigated by performing a parametric study that documented the effects on delay and attenuation of the rebar reflection for specific material property values.

Model 2 can help explain some of the accuracy issues documented during GPR investigations of bridge decks. In this model, the rebar are not necessarily in contact with contaminants in the bridge deck, which may result in damage being reported when in fact the rebar is surrounded by sound concrete. Further, the surface reflection is not necessarily increased in areas of high contamination in Model 2, which may cause some damaged areas to be missed. There is little doubt that at some point in the deterioration process the rebar is surrounded by contaminated material that may extend up to the surface. However, it is difficult to discern this state in GPR data from the conditions proposed in Model 2, which is likely to occur early in the deterioration process. In addition, the parameters of Model 2 are dependent on environmental factors that dictate how much moisture has penetrated into the deck at

the time of the GPR survey. Sound concrete may appear contaminated after a rainstorm and deteriorated concrete may appear sound after a stretch of hot, dry weather.

The first step in improving the accuracy of GPR bridge deck surveys is to understand why errors in data interpretation occur. The material models examined in this thesis contribute to that understanding. One area of future work is to find empirical evidence to validate the models formulated here, as well as to identify what ranges of material property values are typical. This may offer insight on how to tell the difference between early and advanced stages of deterioration in GPR data.

References

ASCE. (2009). *Report Card for America's Infrastructure*. Retrieved 2 9, 2011, from American Society of Civil Engineers: http://www.infrastructurereportcard.org/

ASNT. (2011). *American Society for Nondestructive Testing*. Retrieved 3 23, 2011, from Introduction to Nondestructive Testing: http://www.asnt.org/ndt/primer1.htm

Barnes, C. L., & Trottier, J.-F. (2004). Effectiveness of Ground Penetrating Radar in Predicting Deck Repair Quantities. *Journal of Infrastructure Systems* , 69-76.

Barnes, C. L., & Trottier, J.-F. (2000). Ground Penetrating Radar for Network-Level Concrete Deck Repair Management. *Journal of Transportation Engineering* , 257-262.

Barnes, C. L., & Trottier, J.-F. (2002). Phenomena and Conditions in Bridge Decks That Confound Ground-Penetrating Radar Data Analysis. *Transportation Research Record* , 57-61.

Barnes, C. L., Trottier, J.-F., & Forgeron, D. (2008). Improved Concrete Bridge Deck Evaluation Using GPR by Accounting for Signal Depth-Amplitude Effects. *NDT&E International* , 427-433.

Belli, K. (2008). *Ground Penetrating Radar Bridge Deck Investigations Using Computational Modeling.* 2008: Northeastern University.

Belli, K., Rappaport, C. M., Zhan, H., & Wadia-Fascetti, S. (2009). Effectiveness of 2-D and 2.5-D FDTD Ground-Penetrating Radar Modeling for Bridge-Deck Deterioration Evaluated by 3-D DFTD. *IEEE Transactions on Geoscience and Remote Sensing* , 3656-3663.

Belli, K., Rappaport, C., & Wadia-Fascetti, S. (n.d.). A Time Domain Equivalent Source Model of an Impulse GPR Antenna Based on Measured Radiation Fields. *accepted for publication in Research in Nondestructive Evaluation* .

Belli, K., Rappaport, C., & Wadia-Fascetti, S. (2009). Forward Time Domain Ground-Penetrating Radar Modeling of Scattering from Anomalies in the Presence of Steel Reinforcements. *Research in Nondestructive Evaluation , 20*, 193-214.

Belli, K., Wadia-Fascetti, S., & Rappaport, C. (2011). Integrated Sensor and Media Modeling Environment Developed and Applied to Ground-Penetrating Radar Investigation of Bridge Decks. *Journal of Computing in Civil Engineering* , 10-20.

Belli, K., Wadia-Fascetti, S., & Rappaport, C. (2008). Model Based Evaluation of Bridge Decks Using Ground Penetrating Radar. *Computer-Aided Civil and Infrastructure Engineering* , 3-16.

Buyukozturk, O. (1997). Electromagnetic Properties of Concrete and Their Significance in Nondestructive Testing. *Transportation Research Record* , 10-17.

Cartz, L. (1995). *Nondestructive Testing.* Materials Park, OH: ASM International.

Elbeltagi, E., & Tantawy, M. (n.d.). *Asset Management: The Ongoing Crisis.* Retrieved 2 10, 2011, from Mansoura University: http://app2.mans.edu.eg/eulc/Libraries/itemsAttach/IssueArticle/2804/Asset%20Crisis-Saudi08.pdf

Firoozabadi, R., Miller, E. L., Rappaport, C. M., & Morgenthaler, A. W. (2007). Subsurface Sensing of Buried Objects Under a Randomly Rough Surface Using Scattered Electromagnetic Field Data. *IEEE Transactions on Geoscience and Remote Sensing , 45*, 104-117.

Gontar, W. A., Martin, J. P., & Popovics, J. S. (2000). Effects of Cyclic Loading on Chloride Permeability of Plain Concrete. In F. Ansari (Ed.), *Condition Monitoring of Materials and Structures* (pp. 95-107). Reston, VA: American Society of Civil Engineers.

GSSI. (2011). *Road Inspection Antennas*. Retrieved 3 7, 2011, from Geophysical Survey Systems Incorporated: http://www.geophysical.com/roadscan.htm

Halabe, U. B. (1990). *Condition Assessment of Reinforced Concrete Structures Using Electromagnetic Waves.* Cambridge, MA: Massachusetts Institute of Technology.

Hegazy, T., Elbeltagi, E., & Elbehairy, H. (2004). Bridge Deck Management System with Integrated Life Cycle Cost Optimization. *Transportation Research Record: Journal of the Transportation Research Board* , 44-50.

Hellier, C. J. (2003). *Handbook of Nondestructive Evaluation.* McGraw-Hill Professional Publishing.

Maser, K. (1991). Bridge Deck Condition Surveys Using Radar: Case Studies of 28 New England Decks. *Tranportation Research Record* , 94-102.

Maser, K. R. (1996). Condition Assessment of Transportation Infrastructure Using Ground-Penetrating Radar. *Journal of Infrastructure Systems* , 94-101.

Maser, K. R., & Rawson, A. (1992). Network Bridge Deck Surveys Using High-Speed Radar: Case Studies of 44 Decks. *Transportation Research Record* , 25-28.

McCann, D. M., & Forde, M. C. (2001). Review of NDT Methods in the Assessment of Concrete and Masonry Structures. *NDT&E International* , 71-84.

Nielson, E. P., & Geiker, M. R. (2003). Chloride Diffusion in Partially Saturated Cementitious Material. *Cement and Concrete Research* , 133-138.

NRMCA. (1995). *Concrete In Practice*. Retrieved January 31, 2011, from National Ready Mixed Concrete Association: http://www.nrmca.org/aboutconcrete/cips/25p.pdf

PCA. (2011). *Portland Cement Association*. Retrieved 1 28, 2011, from Corrosion of Embedded Materials: http://www.cement.org/tech/cct_dur_corrosion.asp

Rappaport, C. M. (2007). Accurate Determination of Underground GPR Wavefront and B-Scan Shape From Above-Ground Point Sources. *IEEE Transactions on Geoscience and Remote Sensing , 45* (8), 2429-2434.

Rappaport, C. M. (2007). Ground Penetrating Radar. In M. Golio (Ed.), *RF and Microwave Engineering Handbook.* Boca Raton: CRC Press.

Rens, K. L., Nogueira, C. L., & Transue, D. J. (2005). Bridge Management and Nondestructive Evaluation. *Journal of Performance of Constructed Facilities* , 3-16.

Romero, F. A., Roberts, G. E., & Roberts, R. L. (2000). Evaluation of GPR Bridge Deck Survey Results Used for Delineation of Removal/Maintenance Quantity Boundaries on Asphalt-Overlaid, Reinforced Concrete Deck. *Structural Materials Technology: An NDT Conference*, (pp. 23-30). Atlantic City, NJ.

Sadiku, M. N. (2001). *Numerical Techniques in Electromagnetics.* CRC Press LLC.

Sbartai, Z. M., Laurens, S., Balayssac, J.-P., Arliguie, G., & Ballivy, G. (2006). Abilty of the Direct Wave of Radar Ground-Coupled Antenna for NDT of Concrete Structures. *NDT&E International* , 400-407.

Shull, P. J. (2002). *Nondestructive Evaluation.* New York, NY: Marcel Dekker, Inc.

Society of Exploration Geophysicists of Japan. (1998). *Handbook of Geophysical Exploration.*

von Hippel, A. (1954). *Dielectric Materials and Applications.* Cambridge, MA: Technology Press of MIT.

Xi, Y., & Bazant, Z. P. (1999). Modeling Chloride Penetration in Saturated Concrete. *Journal of Materials in Civil Engineering* , 58-65.

Zhan, H., Rappaport, C., Farid, M., Alshawabkeh, A., & Raemer, H. (2007). Born Approximation Modeling of Lossy Soil Half-Spaces for Cross-Well Radar Sensing of Contaminants with Low-Order Parameter. *IEEE Transactions on Geoscience and Remote Sensing* , 2423-2429.